Spin-up from rest in a stratified fluid: boundary flows

By JAN BERT FLÓR[1], MARIUS UNGARISH[2]
AND JOHN W. M. BUSH[3]

[1]Laboratoire des Ecoulements Géophysiques et Industriels (LEGI),
CNRS-INPG-UJF, BP 53X, 38041 Grenoble, France
[2]Department of Computer Science, Technion, Haifa, Israel
[3]Department of Mathematics, MIT, Cambridge, MA 01239, USA

We present the results of an integrated experimental, numerical and theoretical examination of spin-up from rest of a stratified fluid. A vertical cylindrical container of radius R and height $2H$ containing fluid of viscosity v and characterized by a constant buoyancy frequency N is set impulsively to rotate about its symmetry axis with angular speed $\Omega = f/2$. The characteristic Ekman number $E = v/\Omega R^2$ is small and the Schmidt number $S = v/D_s$ (where D_s is the diffusivity of salt) is large. The investigation is focused on elucidating the initial stage of spin-up, which is characterized by an axisymmetric circulation driven by nonlinear Ekman layers adjoining the horizontal boundaries. Fluid is drawn by the boundary layers from the stationary, stratified interior and transported into corner regions. It is shown that the corner regions are restricted to a height of approximately $0.3Rf/N$ from the horizontal boundaries, above which the fluid remains unperturbed apart from that spun up by diffusion of momentum from the sidewall boundary. Two distinct regions thus emerge: rotating corner regions, and a quiescent stratified core. After a time $1.3/(E^{1/2}N)$, the corner regions cover the bulk of the horizontal boundaries and the boundary layer suction is suppressed. Our study provides a framework for understanding the subsequent evolution of the spin-up process, which may be characterized by axisymmetry-breaking instabilities of the stratified core.

1. Introduction

The spin-up of a stratified fluid represents an important paradigm in geophysical fluid dynamics, as it describes an adjustment process which arises commonly in both the atmosphere and oceans. Oceanographic situations where the dynamics of stratified spin-up is important include wind-stress-driven flows in both the open ocean and coastal regions (Pedlosky 1968; Blumsack 1972; Anderson & Gill 1975; Dewar, Rhines & Young 1984; Spence, Foster & Davies 1992). The physical processes accompanying stratified spin-up also play a role in the dynamics of ocean vortices, for example meddies (McWilliams 1985), arctic eddies (Manley & Hunkins 1985), and megaplume hydrothermal emissions (Baker 1995). Finally, spin-up effects arise in a variety of industrial processes, for example centrifugal separation (Ungarish 1993). A comprehensive review of spin-up in homogenous and stratified fluids has recently been presented by Duck & Forster (2001).

Spin-up is the generic term used to describe the adjustment of a bound fluid system

in response to a change in rotation rate of its container from $\Omega - \Delta\Omega$ to Ω. When the fluid is homogeneous, the adjustment is between two states of solid body rotation. The simplest case is that of a cylindrical container of height $2H$ and radius R rotating about its axis of symmetry (defined to be the z-direction) in which the Ekman number, $E = \nu/(\Omega R^2)$, is sufficiently small that the dynamic influence of viscosity is confined to thin boundary layers adjoining the container walls. When the Rossby number $Ro = \Delta\Omega/\Omega$ is small, the flow may be described by linear theory: Ekman layers on the upper and lower surfaces transport fluid from the geostrophic interior into the vertical shear layers adjoining the vertical walls, which return the spun-up fluid to the interior (Greenspan & Howard 1963). Throughout this process, the bulk interior is described by a geostrophic balance, so that its angular velocity is independent of z to leading order, in compliance with the Taylor–Proudman theorem: the spin-up arises only by virtue of the secondary $O(E^{-1/2})$ flow generated by the Ekman boundary layers on the horizontal bounding walls. Continuity requires that there be an associated $O(E^{-1/2})$ meridional inflow within the bulk interior. Conservation of angular momentum requires that the fluid's angular velocity increase as it is transported radially inward. The angular velocity of the fluid thus adjusts to that of the boundaries after a net radial displacement of $O(RRo)$ and a spin-up timescale $\tau_s \sim \Omega^{-1}E^{-1/2}(2H/R)$ (Greenspan 1968).

Spin-up from rest ($Ro = 1$) is a more complex, inherently nonlinear process (Wedemeyer 1964; Weidman 1976a, b). The fluid is initially without angular momentum, and so may acquire it exclusively through viscous interaction with the rigid boundaries. The boundary layers assume the form of nonlinear Ekman layers (closely related to von Kármán layers), through which all the fluid must be flushed in order to achieve spin-up. The analysis of Wedemeyer (1964) and Weidman (1976a, b) indicates that, as in the linear case, the angular velocity in the core remains z-independent throughout the spin-up process, which is achieved, again, over a timescale $\tau_s \sim \Omega^{-1}E^{-1/2}(2H/R)$. In nonlinear spin-up, however, boundary layer instability may serve to enhance the transfer of angular momentum from the boundaries to the fluid bulk, and so to expedite the spin-up process.

When the fluid is initially stratified, the spin-up process is considerably more complex. Strictly speaking, no quiescent state can exist in a rotating stratified fluid: curvature of the isopycnals results in diffusive mass transport with a radial component, and the concomitant Sweet–Eddington azimuthal flow. Stratified spin-up thus typically refers to the adjustment of the fluid from one dynamic state to another: the final flow will generally depend on the final density profile, and will be strictly quiescent (in the rotating system) only if the fluid is completely homogenized by mixing or diffusive processes. Almost all studies of stratified spin-up have focused on the linear (or 'secular') case, in which $Ro \ll 1$ (Holton 1965; Pedlosky 1967; Walin 1969; Sakurai 1969; Buzyna & Veronis 1971; Hyun, Fowlis & Warn-Varnas 1982; St-Maurice & Veronis 1975; Beardsley *et al.* 1979; see also Spence *et al.* 1992). Owing to its relevance in transient geophysical flows, a number of recent studies have been directed towards understanding stratified spin-up over sloping topography (MacCready & Rhines 1991), where the non-zero component of buoyancy along the boundary layer complicates the analysis and may result in an unsteady boundary layer. Duck, Foster & Hewitt (1997) and Hewitt *et al.* (1999) consider stratified spin-up in a conical container, and explore both linear and nonlinear regimes.

The problem of nonlinear stratified spin-up from rest in a cylindrical container has received comparatively little attention. Greenspan (1981) presented the results of a qualitative experimental investigation of the problem, but did not present any

supporting theoretical developments. Hyun (1983) presented finite-difference numerical solutions for a thermally stratified Boussinesq fluid, but without experimental or analytical support. Present observations have shown that the evolution of stratified spin-up from rest can be characterized by two distinct stages. The first stage is purely axisymmetric, and dominated by the generation of corner regions through radial boundary layer transport. These corners expand radially inwards towards the centre until rotating fluid covers the top and bottom boundaries. The subsequent evolution depends explicitly on N/f and H/R. For small f/N, the interior spins up by the viscous diffusion of momentum from the container boundaries, and the flow maintains its axisymmetry. For large f/N, the core region typically becomes unstable and loses its axial symmetry, in a manner described qualitatively by Greenspan (1981).

In this paper we investigate the first stage, a process common to all observed modes of stratified spin-up from rest, specifically the establishment and growth of the corner regions by boundary layer transport towards and along the horizontal bounding surfaces. Although the second stage is rich and challenging from the point of view of stability, it is clear that the analysis of the first stage is an essential prerequisite to understanding the subsequent evolution. In particular, the first stage determines the initial conditions required for an assessment of the stability of the non-rotating core. The second stage will be investigated in a forthcoming paper.

The goal of our work is to develop a fundamental understanding of the initial stage of stratified spin-up from rest by using a combination of laboratory experiments, numerical simulations and analytical modelling. The paper is organized as follows. Our experimental methods and observations are described in §2. In §3, we describe our supporting numerical simulations and results. Based on insights provided from our experimental observations and numerical simulations, we develop an analytical model of stratified spin-up from rest in §4. In §5, we demonstrate that the model predictions for the evolution of the corner regions are in good agreement with both our experimental observations and numerical simulations. Concluding remarks and directions of further study are discussed in §6.

2. Experimental study

2.1. *Apparatus*

A schematic illustration of the experimental apparatus is presented in figure 1. The cylindrical tank was filled with a linearly stratified saltwater solution using the Oster double-bucket technique. In order to avoid optical distortion by the curved sidewalls, the cylindrical tank was submerged in a 1×1 m square Perspex container filled with tap water. The tanks were positioned on a 1 m diameter rotating platform equipped with a vertical neon–argon laser sheet that was stable in the rotating frame of reference. Density measurements were made with a high-resolution conductivity probe (Precision Measurement Engineering) mounted on a mechanical traverse that allowed vertical sampling through the fluid domain.

After the tank was filled, a metal frame spanned by horizontal cotton wires coated with dried fluorescein dye was carefully placed in the fluid. As the fluorescein dye dissolved, the metal frame was slowly turned, generating horizontal planes of dyed fluid of typical thickness 2 mm. This method allows clear visualization of the vertical motions of the dye planes which correspond to isopycnal surfaces. The frame was removed and a horizontal lid placed at the free surface.

Before the rotation was initiated, the vertical density profile was measured, and the
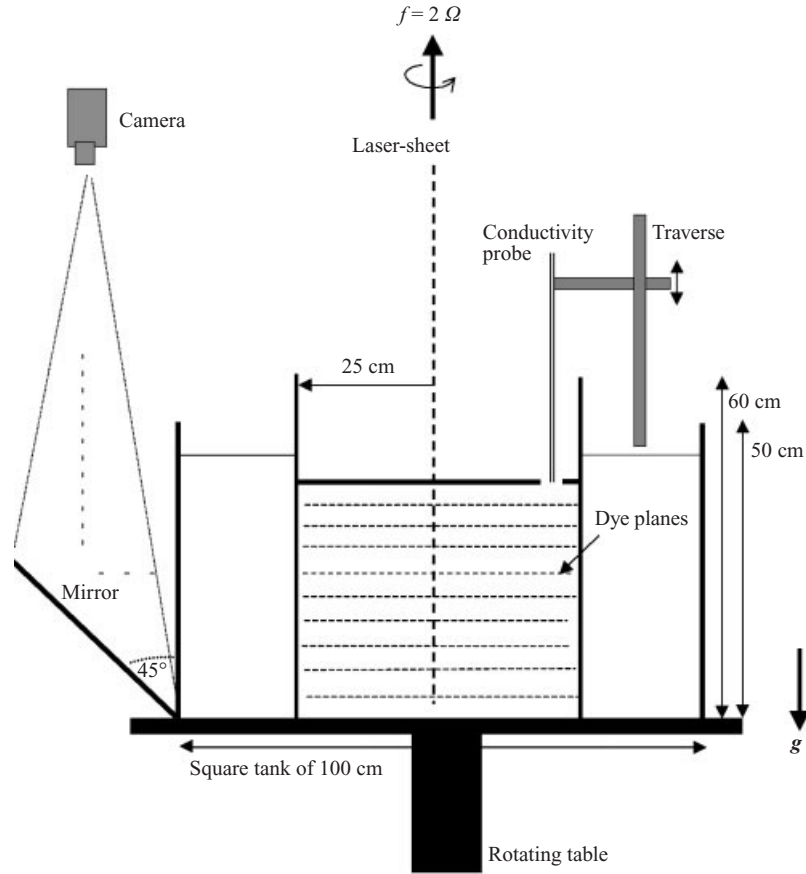
FIGURE 1. A schematic illustration of the experimental apparatus.

Brunt–Väisälä frequency $N = [-(g/\rho)(\partial\rho/\partial z)]^{1/2}$ calculated, by passing a conductivity probe vertically through the fluid domain (through a hole of 3 cm diameter in the lid approximately 4 cm from the side wall). The table was set into motion, and the angular speed Ω achieved in less than one rotation period. The density profiles were measured before and after the spin-up process. The flow was illuminated by a vertical laser sheet which passed through the tank centreline. An analog camera mounted in the rotating frame recorded the flow evolution and the images were directly recorded on the hard disk of a PC. A typical image obtained just prior to the onset of rotation is shown in figure 2. We note that if the dye is not emplaced horizontally, the rotating field of view erroneously suggests vertical motions within the fluid. For further image processing the software NIH-image for PCs was used.

The $(f/N, H/R)$ parameter regime was explored, with the individual parameter ranges being $0.9 \text{ s}^{-1} \leqslant N \leqslant 2 \text{ s}^{-1}$, $0.1 \text{ s}^{-1} \leqslant f \leqslant 2.2 \text{ s}^{-1}$, $10 \text{ cm} \leqslant H \leqslant 60 \text{ cm}$ and $R = 25 \text{ cm}$. The non-dimensional parameter ranges were $0.4 \leqslant f/N \leqslant 2.5$ and $0.54 \geqslant H/R \geqslant 2$. Observations of the dye field gave information about the boundary layer flows, the instability of the non-rotating core fluid, and a qualitative measure of the mixing of the stratified fluid. Two particular experiments, referred to as A and B, will be discussed in detail and compared with our numerical simulations. The governing parameters in experiments A and B are listed in table 1.

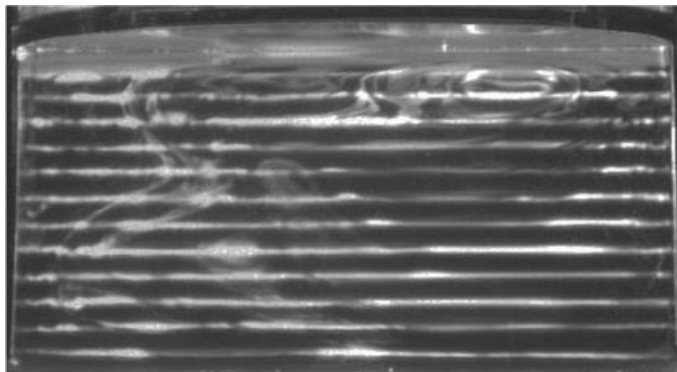| Exp.	N (s^{-1})	Ω (s^{-1})	$2H$ (cm)	R (cm)	f/N	$E = \nu/(\Omega R^2)$
A	1.63	0.305	21.5	25	0.374	5.25E-05
B	1.69	1.02	25.0	25	1.23	1.57E-05

TABLE 1. Governing parameters for experiments A and B.

FIGURE 2. A typical image of a vertical cross-section through the centre of the tank prior to the onset of rotation. Note the horizontal fluorescein dye planes whose vertical motion reflects that of the isopycnals.

2.2. *Observations*

We first note that the flow in the cylindrical tank was approximately symmetric about the midplane of the tank; consequently, it suffices to describe the flow evolution in the lower half of the tank.

When the tank is set into motion, dense fluid adjacent to the lower boundary is accelerated and experiences a centripetal force that drives radial outflow within a thin von Kármán or nonlinear Ekman boundary layer. This radial flow eventually collides with the sidewall and is ejected vertically until reaching a maximum height limited by the ambient stratification: the spun-up fluid is thus confined to the corners of the container. A corner region with a relatively flat top is evident in figure 3(*a*) at $\Omega t = 10$. Continuity requires that the fluid expelled radially in the boundary layer be replaced by overlying fluid through the action of boundary layer suction. The density of the fluid thus drawn into, and ejected radially by, the lower boundary layer necessarily decreases with time. The corner regions expand toward the centre of the tank, thus progressively decreasing both the area of the central spot where the boundaries are in contact with the non-rotating fluid core, and the momentum of the fluid ejected from the boundary layer. The development of radial stratification within the corner regions by boundary layer transport is necessarily a delicate process, and instability may prompt weak convective overturning of the form evident in figures 3 and 4. Despite this mixing process, whose vigour evidently increases with f/N, a radial stratification clearly emerges (see figure 3*a*, $\Omega t = 20$–50). This process continues until the lower boundary is covered with rotating fluid and the next stage of the spin-up process starts. Finally, we note that the interior fluid above the corner region is largely unperturbed by the boundary-layer-induced circulation, as indicated by the persistence of the horizontality of the local dye lines (figures 3 and 4).

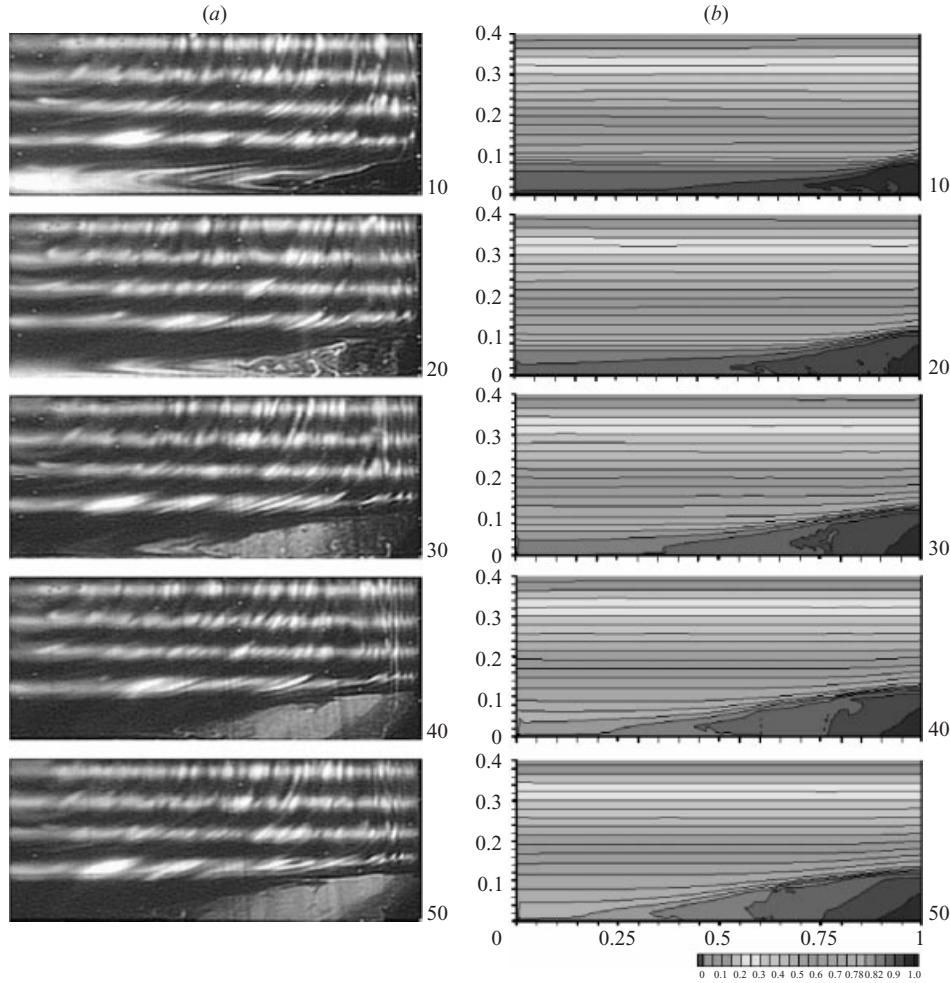Insight into the flow may also be acquired by scrutinizing the evolution of the

FIGURE 3. The evolution of the density field in the lower right quadrant for experiment A. The tank half-height and radius are, respectively, 10 cm and 25 cm and the density varies from $1.032\,\mathrm{g\,cm^{-3}}$ at the top to $1.06\,\mathrm{g\,cm^{-3}}$ at the bottom of the image. The distance between the horizontal dye lines in (*a*) is 2 cm, corresponding to $\delta\rho = 0.0056\,\mathrm{g\,cm^{-3}}$ with the top of the lowest dyeline initially at 2 cm above the bottom. (*a*) Experimental observations and (*b*) numerical simulations of the density field at times $\Omega t = 10, 20, 30, 40, 50$ after the onset of rotation, where $\Omega = 0.305\,\mathrm{s^{-1}}$.

dye patterns. In particular, the shear gives texture to the dye and organizes it into a layered 'onion skin' structure with the layers aligned parallel to the shear. The layers parallel to the wall indicate the diffusion of momentum from the sidewall, while those in the thin region above the slope of the corner region indicate an intense shear (see figure 3*a*, $\Omega t = 30, 40$ and 50). This shear is not aligned with the horizontal dyelines representing the isopycnals, and is therefore susceptible to convective instability. We note that the apparent onion-skin structure evident in the centre of the tank in figure 3(*a*) is simply a remnant generated during the dye preparation and fosilized before starting the experiment.

Though the initial evolution of the flow for strong ($f/N < 1$) and weak ($f/N > 1$) stratifications is similar, some notable differences were evident. For strong stratification, the interface between the corner region and interior fluid is well defined and
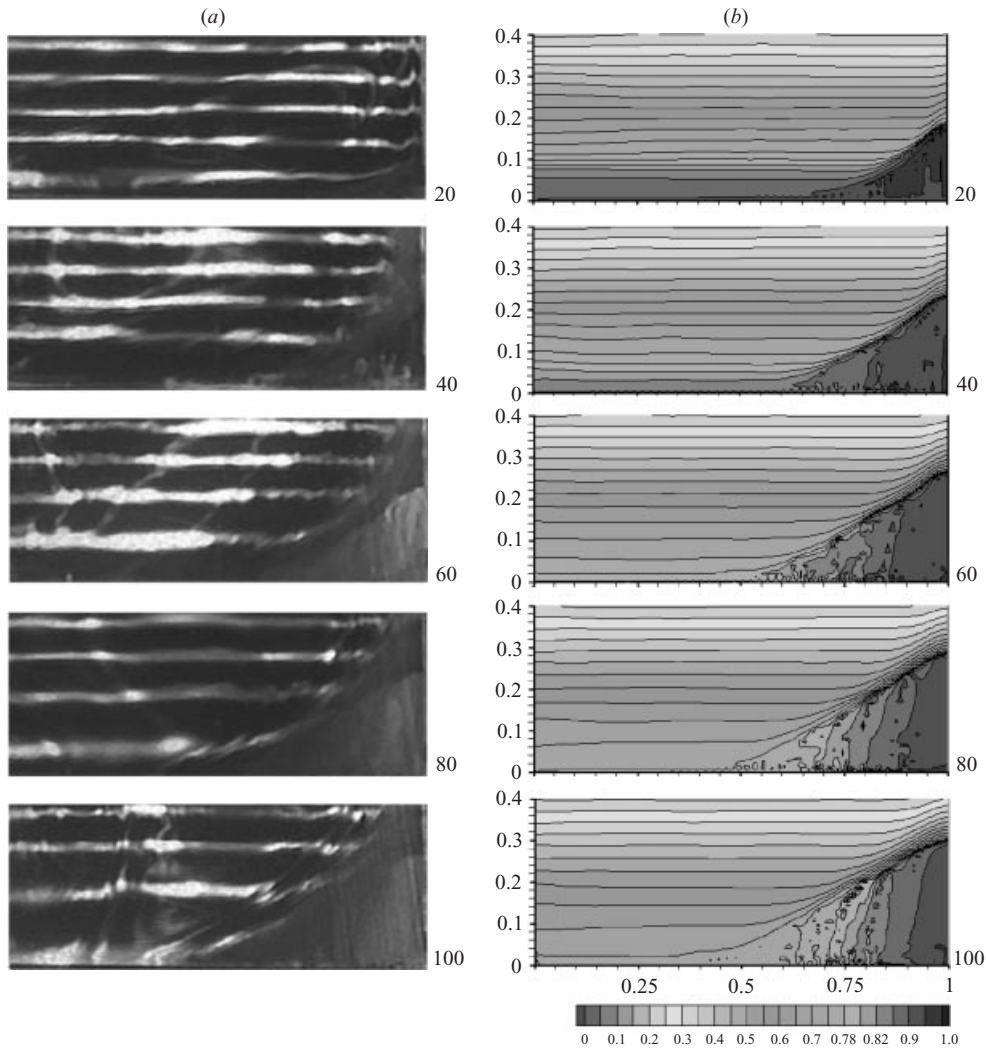
FIGURE 4. The evolution of the density field in the lower right quadrant for experiment B. The tank half-height and radius are, respectively, 10 cm and 25 cm and the density varies from 1.045 g cm^{-3} at the top to 1.075 g cm^{-3} at the bottom of the image. The distance between the horizontal dye lines in (*a*) is 2 cm, corresponding to a $\delta\rho = 0.006$ g cm^{-3}. (*a*) Experimental observations and (*b*) numerical simulations of the density field at times $\Omega t = 20, 40, 60, 80, 100$ after the onset of rotation, where $\Omega = 1.02$ s^{-1}.

weakly inclined relative to the horizontal (figure 3*a*). For weak stratification, the angle of inclination of the interface with the horizontal increases owing to the relative increase of the centrifugal to the buoyancy forces (figure 4*a*). Initially, the interface between the corner region and interior is sharp. Subsequently, baroclinic wave motions develop (see figure 4*a*, $\Omega t = 10$), and increase in amplitude until breaking, thus leading to overturning and local mixing (see figure 4*a*, $\Omega t = 20, 40$ and 60). The wave-induced mixing does not significantly penetrate the underlying corner regions, owing to the substantial density difference between core and corners. Nevertheless, the baroclinic waves may play an important role in exciting the instability of the core fluid in the subsequent flow stage.

At the end of this initial stage, the flow is characterized by an isolated, stationary, vertically stratified core region suspended between the rotating corner regions. The corner regions thus achieve a quasi-steady height determined by the total volume extruded by the boundary layer transport and the pressure distribution within the fluid. Subsequently, fluid adjoining the sidewall boundary gradually spins up by diffusion of momentum, thus reducing the pressure difference between corner regions and the interior. The rotating corner fluid thus eventually slumps back towards the centre of the tank until it covers the entirety of the lower boundary. The detailed evolution of the corner regions in the initial stage will be considered explicitly in § 5, where our experimental observations will be compared with numerical simulations and predictions based on our supporting theoretical model.

Finally, it is noteworthy that the density of the fluid ejected into the upper corner regions increases with time, while that into the lower corners decreases. Thus, in the lower corner the newly accumulated fluid is expected to form a positive $\partial \rho / \partial r$ stratification, while in the upper corner a negative stratification is expected. One thus may infer that in the upper corner the fluid is centrifugally less stable and more susceptible to mixing; however, no striking difference between upper and lower corner regions was observed.

The second stage of the flow evolution was observed to depend explicitly on the aspect ratio of the core, $2H_c/R_c$, and f/N_c, with N_c the stratification of the core fluid. At the end of the initial stage, N_c is necessarily less than the initial N (see figures 3 and 4) owing to the boundary layer flows described herein. When $f/N_c < 1$ and $2H_c/R_c > 1$, the flow maintains its axisymmetry, and the core fluid spins up principally by the viscous diffusion of momentum from the container boundaries. When $f/N_c < 1$ and $2H_c/R_c < 1$, the central core develops an elliptical instability, which results in a series of vertical vortices that more efficiently transfer momentum from the container walls and so expedite the spin-up process. Finally, when $f/N_c > 1$, the aforementioned baroclinic waves evident on the boundaries of the core eventually break, thus prompting the axisymmetry-breaking instability of the central core also reported by Greenspan (1981). This subsequent stage of flow evolution will be the subject of a forthcoming paper.

3. Numerical model

Our experiments indicate that the initial stage of the stratified spin-up process is inherently axisymmetric; moreover, in certain parameter regimes, the axisymmetry is maintained in the subsequent stage. We proceed by detailing our numerical simulations, which enable us to characterize the axisymmetric components of the spin-up process. The description obtained from our experiments is thus complemented by the more detailed information about the velocity and density fields obtained from our numerical simulations.

3.1. *Formulation*

A vertical cylindrical tank of height $2H$ and radius R containing a linearly stratified fluid is set into rotation about its symmetry axis with constant angular speed Ω. We define the cylindrical coordinate system (r, θ, z) in the rotating frame of reference where the z-axis corresponds to the tank centreline and $z = 0$ defines the base of the tank. We denote by $\mathbf{v}$ the fluid velocity relative to the rotating frame, and by $-g\hat{\mathbf{z}}$ the gravitational acceleration. We scale lengths with the container radius, R, velocities

with ΩR and times with Ω^{-1}. We introduce the density function $\phi(\boldsymbol{r}, t)$ by

$$\rho(\boldsymbol{r}, t) = \bar{\rho}[1 + \gamma\phi(\boldsymbol{r}, t)], \tag{3.1}$$

where $\Delta\rho$ is the initial density difference over the tank depth, $\gamma = \Delta\rho/\bar{\rho}$ is the reduced density difference and $\bar{\rho} = \rho(H)$ is the initial density at the midplane of the tank.

The dimensionless balance equations are as follows.

(*a*) Continuity

$$\nabla \cdot \boldsymbol{v} = 0 \tag{3.2}$$

(*b*) Momentum balance

$$\frac{D\boldsymbol{v}}{Dt} + 2\hat{\boldsymbol{z}} \times \boldsymbol{v} = \frac{1}{1 + \gamma\phi}[-\nabla p + \phi(\gamma r\hat{\boldsymbol{r}} - \mathscr{F}^{-2}\hat{\boldsymbol{z}}) + E\nabla^2\boldsymbol{v}], \tag{3.3}$$

where p is the reduced pressure (expressible in terms of the fluid pressure P in dimensional form, $p = P + \bar{\rho}(gz - 0.5\Omega^2 r^2)$). We note that the Boussinesq approximation may be recovered by setting $\gamma = 0$ in (3.3), but that no significant numerical advantage is gained through this approximation.

(*c*) Density transport

$$\frac{D\phi}{Dt} = \frac{E}{\sigma}\nabla^2\phi. \tag{3.4}$$

The relevant dimensionless parameters, in addition to γ, are the aspect ratio H/R (the dimensionless half-height) of the tank, the Ekman number

$$E = \nu/(\Omega R^2), \tag{3.5}$$

the rotational Froude number (squared)

$$\mathscr{F}^2 = \frac{\Omega^2 R}{\gamma g} = \frac{R}{4H}\left(\frac{f}{N}\right)^2, \tag{3.6}$$

and the Schmidt number $\sigma = \nu/D_s$, where D_s is the diffusivity of salt. The aspect ratio of the container is of order unity. We consider flows with very small values of E, small γ and large σ ($\sigma \approx 700$ for saltwater). The typical value of E/σ in the systems under consideration is too small for numerical resolution of density diffusion with affordable computations. Therefore the value $\sigma = 10$ is used here to provide an artificial diffusion coefficient, whose contribution is significant only in the numerical smoothing (over 2–3 grid intervals) of the ϕ-discontinuity interface between the corner region and the interior, and which has a negligible influence on the bulk dynamics.

For simplicity of discussion and reduction of the computational domain we consider only the lower part of the container, $0 \leqslant r \leqslant 1$, $0 \leqslant z \leqslant H$. The symmetry between the upper and the lower regions is expected for the parameter range of interest (specifically, small $\Omega^2 R/g$ and γ), and consistent with our experimental observations. The initial conditions at $t = 0$ are

$$\boldsymbol{v} = -r\hat{\boldsymbol{\theta}}, \tag{3.7}$$

$$\phi = 1 - \frac{z}{H}. \tag{3.8}$$

The boundary conditions for $t \geqslant 0$ are $\boldsymbol{v} = \boldsymbol{0}$ on the bottom and sidewalls, symmetry conditions on the z-axis and midplane $z = H$, and $\partial\phi/\partial n = 0$ on the walls, where n is the normal. In several test cases the velocity boundary conditions at $z = H$ were changed to approximate an open boundary, but the influence on the spin-up process was insignificant.
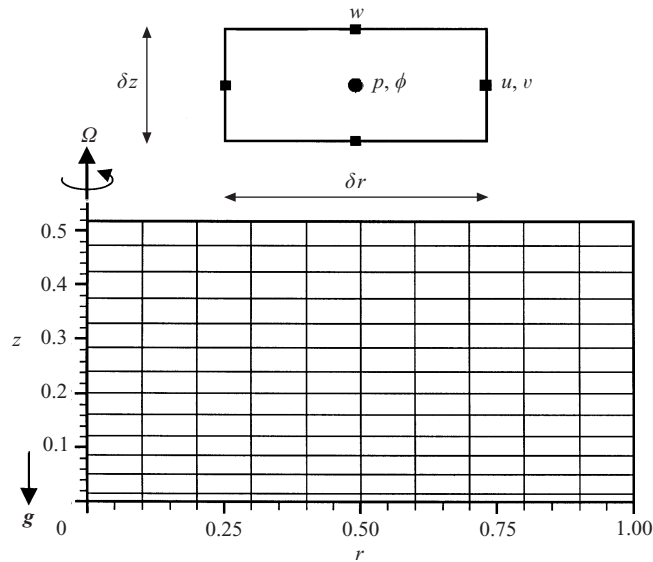
FIGURE 5. Sketch of the staggered grid and computational cell used for the numerical calculations. Here the number of radial intervals $il = 10$, and vertical intervals $jl = 11$. All lengths are scaled with R.

The details of the numerical code employed in our numerical simulations are provided in the Appendix. The numerical solution of (3.1)–(3.4) subject to the afore-mentioned initial and boundary conditions was performed by a numerical code based on a forward-time finite-difference technique. We used the staggered grid sketched in figure 5 with typically $il = 200$ constant radial intervals and $jl = 150$ stretched axial intervals. The mesh intervals were considerably smaller than the typical structures of the flow field under consideration; in particular, at least 3 axial intervals were contained within the Ekman length $E^{1/2}$. The resulting error in the boundary layer transport was less than 1%. The artificial smoothing terms were considerably smaller than E. The salt diffusion layers are beyond the resolution of our grids; however, the diffusion of salt is expected to be negligible over the timescales of interest.

The numerical code was subjected to standard resolution studies and found to provide accurate simulations of the experimental configurations. Finally, the numerical code has been tested on problems of spin-up (differential and from rest) of homo-geneous and two-layer fluids and yields good agreement with independent theoretical and experimental results (see Ungarish & Mang 2003).

3.2. *Simulations*

The evolution of the density fields in the numerical simulations of experiments A and B are displayed in figure 3(b) and figure 4(b), respectively. The numerical frames are captured at times corresponding to those reported in the experiments. Figure 3(b) illustrates the case of $f/N < 1$ and indicates an evolution that is very close to the experimental observations. The numerical results provide more quantitative detail about the evolution of the density field. In particular, the simulations indicate that a radial stratification of approximately 10% of the initial vertical stratification is established in the corner regions. In the case of $f/N > 1$ (figure 4b), the simulations show that the radial stratification established is no less than in the former case: although fewer separate regions form, the density jumps across individual interfaces
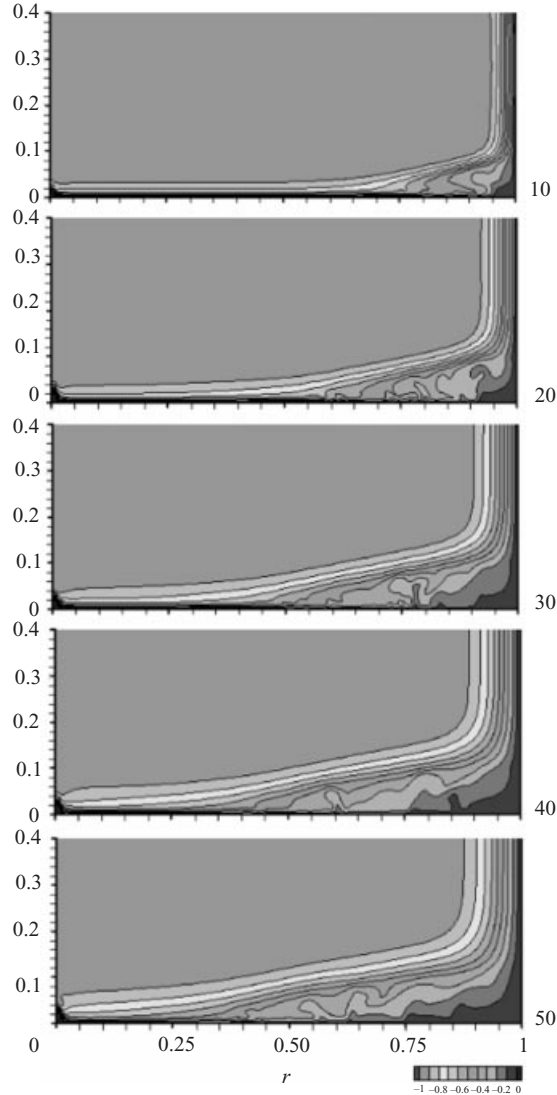
FIGURE 6. Numerical simulations of the evolution of angular velocity $\omega/\Omega - 1$ in experiment A. Here ω is the absolute angular velocity of the fluid. The times shown, $\Omega t = 10, 20, 30, 40, 50$, correspond to those in figure 3.

are larger. Furthermore, in this case the isopycnals are perturbed over a height that extends a considerable distance above the corner region.

An additional quantitative comparison between our experiments and numerical simulations was obtained by tracing the evolution of the radial stratification within the corner regions. In the experiments, each initially horizontal dye plane may be assigned a known density; consequently, provided substantial mixing does not arise, the evolution of the density field may be traced. The density difference between the inner edge of the corner region and the corner were measured at times $\Omega t = 50$ (in experiment A) and 100 (in experiment B), yielding $\delta\rho_A = 0.006 \, \mathrm{g\,cm^{-3}}$ and $\delta\rho_B = 0.012 \, \mathrm{g\,cm^{-3}}$. The corresponding numerically obtained values of $0.0064 \, \mathrm{g\,cm^{-3}}$ and $0.012 \, \mathrm{g\,cm^{-3}}$ for experiments A and B, respectively, show excellent agreement.
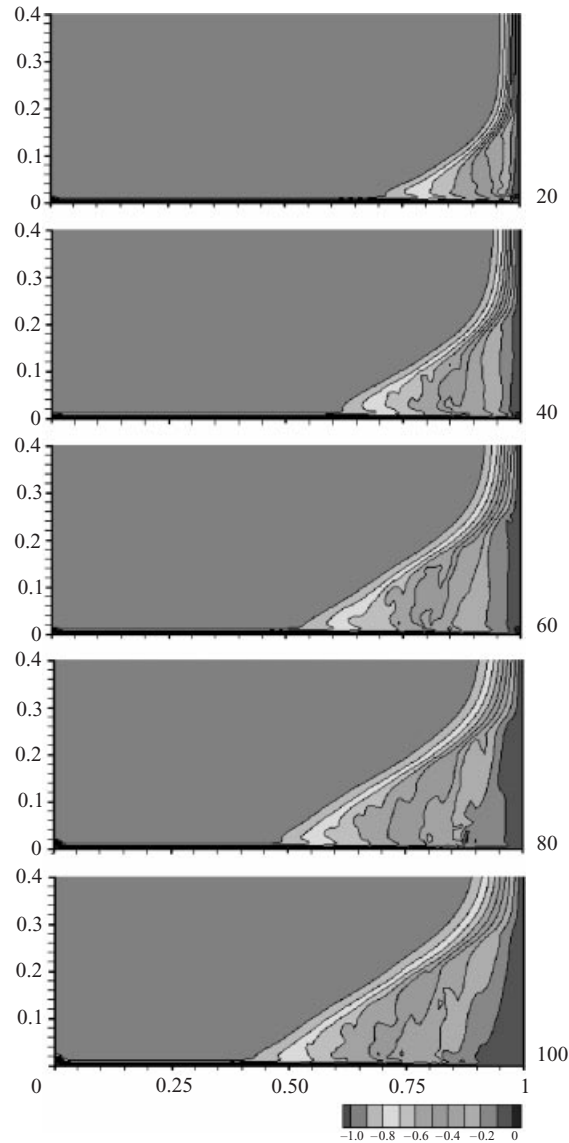
FIGURE 7. Numerical simulations of the evolution of angular velocity $\omega/\Omega - 1$ in experiment B. The times shown, $\Omega t = 20, 40, 60, 80, 100$, correspond to those in figure 4.

The contour plots of angular velocities in the numerical simulations of experiments A and B are displayed in figures 6 and 7, respectively. The simulations reveal a corner region with rotating fluid, an interior core with non-rotating fluid and an intervening shear region that thickens with time. Note that the entirety of the corner regions is not spun-up; rather, the corner region is marked by a radial gradient in angular speed as well as density. Above the corner region, diffusion of vorticity from the sidewall boundary can be observed. This diffusion eliminates the vertical shear across the upper part of the corner region, whose border thus becomes locally horizontal (figures 3a, b and 4a, b). The qualitative behaviour is the same for $f/N < 1$ and $f/N > 1$, but the Ekman transport evidently persists for a longer dimensionless time (i.e. more revolutions of the system) in the latter case.
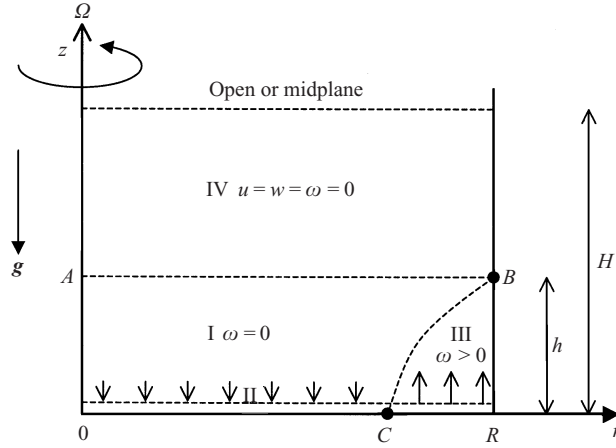
FIGURE 8. Sketch of the idealized model configuration for the lower right quadrant of the fluid domain. Four distinct flow domains are shown. Fluid from the interior domain I is sucked layerwise into the Ekman boundary layer II and ejected into the corner region III, which is separated from I by the interface *BC*. The motion of *BC* compensates for the fluid transferred from region I to III. Region IV remains quiescent, and interface AB does not move.

4. Analytical model

We proceed by presenting a simplified theoretical model, of the momentum-integral type, that describes the initial axisymmetric stage of the spin-up from rest of a stratified fluid. The model attempts to capture the major qualitative features of the flow and to provide some quantitative estimates of the changes which occur in the density and velocity field. Particular attention is given to describing the evolution of the size and shape of the corner region. We propose this model as the stratified-fluid counterpart of Wedemeyer's (1964) classical description of the homogeneous case (see also Greenspan 1968 and Hyun *et al.* 1983).

We consider the configuration detailed in §3.1 and describe all variables in dimensional form unless stated otherwise. The flow field is described in terms of four distinct domains (see figure 8). Domain I contains the original, non-rotating fluid which is drawn downward by suction into the lower boundary layer (domain II). Domain III is the corner region which contains the rotating fluid effluxed radially by the boundary layer. Domain IV contains fluid which is in absolute rest, unperturbed by the rotation of the boundaries. We assume that viscous effects are confined to Ekman-layer-type region II (the contribution of the viscous effects in other regions is reconsidered later). This physical picture is expected to be valid following the establishment of the Ekman layer and corner region (i.e. after several rotation periods), and until the area of contact between region I and the Ekman layer is lost.

The basic circulation is as follows. The Ekman-type boundary layer below domain I draws in fluid. The suction velocity can be approximated by the von Kármán layer result,

$$\tilde{w} = -0.9E^{1/2}\Omega R \quad (0 \leqslant r \leqslant r_F(t), z = 0+), \tag{4.1}$$

where $r_F(t)$ is the innermost position of the spin-up 'front'. This fluid is quickly transfered radially within region II and effluxed at the bottom of domain III. The stratification restricts the axial motion: the effluxed fluid can only penetrate to a limited height. Consequently, region III has a relatively small and quasi-constant maximal height, $h < H$, and must expand inward to accommodate the fluid pumped

in by the boundary layer. The expansion of region III displaces the fluid of region I, whose volume is diminished by the boundary layer suction. Domain IV remains largely unaffected by the flow in regions I–III.

There is evidence (see Hyun *et al.* 1983) that the approximation used by Wedemeyer (1964) provides a good description of spin-up from rest in a homogeneous ambient fluid under certain conditions, which, in the present context, can be expressed as $E^{1/2} \ll h/R$ and $(h/R)^{1/2}E^{1/4} \ll 1$. We assume that these restrictions are fulfilled. Moreover, it can be shown that stratification has a negligibly small, $O(EN^2/f^2)$, contribution to the Ekman layer flow. Consequently, we use a model of Ekman-layer transport that is analogous to that employed in Wedemeyer's approximation. We note that subsequent attempts to refine Wedemeyer's model of nonlinear spin-up from rest in a homogeneous fluid have yielded little, if any, progress.

The underlying idea of the present approximation is the matching of the flow regions I–III as follows. We first postulate a velocity field in region I consistent with the suction boundary condition (4.1), then calculate the corresponding kinematic shape of the interface BC and the density and pressure fields. We then transport the pertinent results into region III, calculate the pressure in domain III, and then use the dynamic pressure continuity condition to match the regions I and III in order to obtain the corresponding 'dynamic' interface. Essentially, this process may be iterated until satisfactory agreement between the kinematic and dynamic shapes of the interface (and other integral properties) is achieved – but the procedure is expected to become extremely cumbersome beyond the first iteration. In the present study, we perform only one step; therefore, useful results can be expressed in a simple analytical form. Due to a carefully chosen initial conjecture, we are able (*a*) to satisfy global volume and mass continuity and obtain a good approximation for the pressure distribution in the radial and axial momentum equations, and (*b*) to show that the kinematic and dynamic loci of the interface are in fair agreement. In addition, we claim that the results are satisfactory on the basis of fair agreement with our numerical solutions and experiments.

Consider the transport equation of the density function (see (3.4)),

$$\frac{\partial \phi}{\partial t} + u\frac{\partial \phi}{\partial r} + w\frac{\partial \phi}{\partial z} = 0. \tag{4.2}$$

The solution of (4.2) by the method of characteristics can be expressed simply as

$$\phi = \text{const on a pathline}, \tag{4.3}$$

subject to the initial condition (3.8). This result has important consequences in the process under investigation. We shall see that the Ekman-layer spin-up circulation induces significant changes in the density distribution in regions I and III, but that region IV remains, again, unperturbed. The neglected diffusion term on the right-hand side of (4.2) is $O(E/\sigma)$ and becomes significant only at very large times or at very sharp density interfaces, descriptions of which are beyond the scope of the present model.

4.1. *Domain I*

We start by choosing a simple non-rotating flow field which satisfies the expected boundary condition at $z = 0$ (the compatibility condition (4.1)) and at $z = h$ (no motion) and the equation of continuity. In addition, we assume that the resulting pathlines of the particles which were initially at the outer wall $r = R$ are of the form of line BC in figure 8. These considerations lead us to the conjecture that the velocity

field in region I is approximately described by

$$u = -0.9E^{1/2}\Omega R\frac{1}{h^2}(h-z)r, \tag{4.4}$$

$$w = -0.9E^{1/2}\Omega R\frac{1}{h^2}(h-z)^2, \tag{4.5}$$

where h is a parameter that will be determined from the matching conditions with region III. The relative simplicity of this velocity field enables us to make further analytical progress; we note that other candidates have been tried and discarded on the basis of this consideration.

We assume that h is time independent, noting that the model does not describe the initial establishment of the corner regions and Ekman layer. Our model describes the subsequent quasi-steady flow in which h evolves very slowly in time (as evidenced in figures 3, 4 and 11, 12). Integrating equation (4.5) we obtain the relation for the vertical displacement $dz = w\,dt$ of a particle. If the vertical position of the fluid particle at time t is z, its initial position at $t = 0$ was z_0, given by

$$z_0(z, T) = h\left[-\frac{1-T}{T} + \frac{h}{T}\frac{1}{-Tz + h(1+T)}\right], \tag{4.6}$$

where

$$T = 0.9E^{1/2}\frac{R}{h}\Omega t \tag{4.7}$$

is the pertinent dimensionless time coordinate of the process.

Since the vertical displacement of a particle in region I is independent of its radial position we conclude, based on (4.3), that the density function in region I remains independent of r. More specifically,

$$\phi(r, z, t) = \phi(z, t) = 1 - \frac{z_0(z, T)}{H}, \tag{4.8}$$

with $z_0(z, T)$ given explicitly by (4.6). In particular, at the base of the tank

$$\phi(r, z = 0, t) = 1 - \frac{h}{H}\frac{T}{1+T}. \tag{4.9}$$

The foregoing velocity and density fields are consistent with the radial and vertical momentum equations. The dominant balance, for small values of the parameter $E^{1/2}R/h$, is simply the hydrostatic pressure corresponding to the instantaneous density distribution,

$$P_I(r, z, t) = -g\int_0^z \left\{\bar{\rho} + \Delta\rho\left[1 - \frac{z_0(z', T)}{H}\right]\right\}dz' + C \tag{4.10}$$

after use of (4.8). Substitution of (4.6) and some algebra yield

$$P_I(r, z, t) = -g(\bar{\rho} + \Delta\rho)z - g\Delta\rho G\left(\frac{z}{h}\right) + C, \tag{4.11}$$

where

$$G(x) = \frac{h^2}{HT}\left[(1-T)x + \frac{1}{T}\ln\left(1 - x\frac{T}{1+T}\right)\right].$$

The line BC in figure 8 represents the locus of the fluid particles which at $t = 0$ were at $r = R$. Integration and some manipulation of the trajectories imposed by (4.4)

and (4.5) yield the following kinematic relationships. First, the equation of BC can be expressed as

$$\frac{z}{h} = 1 + \frac{1}{T}\left(1 - \frac{R}{r}\right), \tag{4.12}$$

and the intersection of BC with the bottom occurs at a radius

$$r_C = R(1 + T)^{-1}. \tag{4.13}$$

Second, the volume of fluid displaced by the motion of BC is given by

$$\Delta V_I = \pi h R^2 \frac{T}{1 + T}; \tag{4.14}$$

this is of course also the volume drawn into the Ekman layer beneath region I during time T. Finally, we calculate the mass removed from the initial region I by the Ekman suction. We obtain

$$\Delta M_I = -\pi \int_0^T \rho(z = 0, T')\tilde{w}r_C^2 \, \mathrm{d}T'$$

$$= (\bar{\rho} + \Delta\rho)\Delta V_I - \frac{\pi}{2}\Delta\rho\frac{h^2}{H}\left(\frac{T}{1 + T}\right)^2 R^2. \tag{4.15}$$

We note that, at $T = 1$, half of the initial fluid of region I has been flushed through the Ekman layer, but at this time the suction of the Ekman layer is already restricted to only 25% of its initial area πR^2.

4.2. *Domain III*

This is the corner region into which the Ekman layer ejects the fluid extracted from region I. Here the fluid rotates with absolute angular velocity $\omega(r, z, t)$ of the order of magnitude of Ω, but the meridional circulation, induced by the Ekman-layer transport, is typically smaller by a factor of $E^{1/2}$. Therefore, to leading order in this small parameter, the momentum balance in the core is described by the cyclostrophic and hydrostatic balances, respectively,

$$-\rho\omega^2 r = -\frac{\partial P}{\partial r}, \tag{4.16}$$

$$0 = -\frac{\partial P}{\partial z} - \rho g. \tag{4.17}$$

The expected density profile is z-independent, as discussed below. In addition, we argue that in the limit of a homogeneous fluid, $\rho = \bar{\rho} = \mathrm{const}$, the angular velocity should reduce to the classical result of Wedemeyer (1964). Therefore, the angular velocity function that satisfies (4.16) and (4.17) may be expressed as

$$\omega^2(r, z, t) = \left\{\frac{1}{1 - A(t)}\left[1 - A(t)\left(\frac{R}{r}\right)^2\right]\right\}^2 \Omega^2 - g\frac{1}{\bar{\rho}}\frac{\partial\rho}{\partial r}(z/r), \tag{4.18}$$

where $A(t) = (r_F/R)^2$ and $r_F(t)$ is the radial position in the Ekman layer where the axial velocity changes sign (from suction to pumping) and the fluid above the Ekman layer changes from stationary to rotating. Ideally, r_F is identical to r_C, the intersection of line BC with the bottom.

The angular velocity provided by equation (4.18) satisfies stringent physical conditions: it encorporates the assumptions of cyclostrophic and hydrostatic balance,

reproduces the expected 'thermal wind' effect (the last term on the right-hand side), and predicts the Ekman-layer efflux which exactly balances the influx from region I. The validity of the assumed form of (4.18) will be highlighted later via comparison with the numerical results. In particular, we shall see that it predicts correctly, both qualitatively and quantitatively, the behaviour of the total angular momentum and frictional torque as functions of time. The formal justification of (4.18), however, is a difficult task left for future investigators.

The rotation in domain III creates a radial pressure gradient. The Ekman bottom layer absorbs the most dense fluid of domain I and ejects it into domain III. (The Ekman layer is very thin and the density variations inside it are negligible.) Since the density of the bottom fluid in region I decreases with time (see (4.9)), so too does the fluid ejected into domain III, where a radial stratification necessarily appears and prevails. We model this feature by

$$\rho = \bar{\rho} + \Delta\rho \left[1 - \frac{h}{H} \frac{T}{1+T} \chi \left(\frac{R-r}{R-r_F} \right) \right], \tag{4.19}$$

where

$$\chi(x) = 2x - x^2. \tag{4.20}$$

The justification for the choice of the function $\chi(x)$ is: (*a*) $\chi(0) = 0$ and $\chi(1) = 1$ reproduce the expected values of ρ at the positions R and r_F, and (*b*) this function satisfies mass conservation between regions I and III (see (4.15)).

We proceed by estimating the pressure distribution in domain III using the radial and axial momentum equations. For small values of the parameters $E^{1/2}R/h$ and $\Delta\rho/\bar{\rho}$, and on account of the angular velocity and density profiles given above, we obtain

$$P_{III}(r, z, t) = -g(\bar{\rho} + \Delta\rho)z + g\Delta\rho\chi \left(\frac{R-r}{R-r_F} \right) \frac{h}{H} \frac{T}{1+T} z$$

$$+ \frac{1}{2}\Omega^2 R^2 \bar{\rho} \left\{ \left[F\left(\frac{r}{R}\right) - F\left(\frac{r_F}{R}\right) \right] \right\} + C, \tag{4.21}$$

where

$$F(x) = \frac{1}{(1-A)^2} \left(x^2 - 2A \ln x^2 - \frac{A^2}{x^2} \right).$$

4.3. *Matching of domains I and III*

The density difference across the interface creates an imbalance between the reduced gravity and centrifugal buoyancy. An order-of-magnitude analysis indicates that an adjustment motion on a relatively short timescale takes place until pressure continuity is achieved. Thus, for the flow field with velocity scales and timescales relevant to the spin-up process, the appropriate condition at the interface BC is pressure continuity.

Let $z = hS(r, T)$ denote the interface between domains I and III, so that at any time T the value of S varies between 0 to 1. This locus is determined by the pressure continuity condition, i.e. $P_I = P_{III}$ along the interface. Using (4.11) and (4.21) we obtain, after some rearrangement,

$$-\frac{2h^2}{T} \left[\chi \left(\frac{R-r}{R-r_F} \right) \frac{T^2}{1+T} S + (1-T)S + \frac{1}{T} \ln \left(1 - \frac{ST}{1+T} \right) \right]$$

$$= C_1 \left[F\left(\frac{r}{R}\right) - F\left(\frac{r_F}{R}\right) \right], \tag{4.22}$$
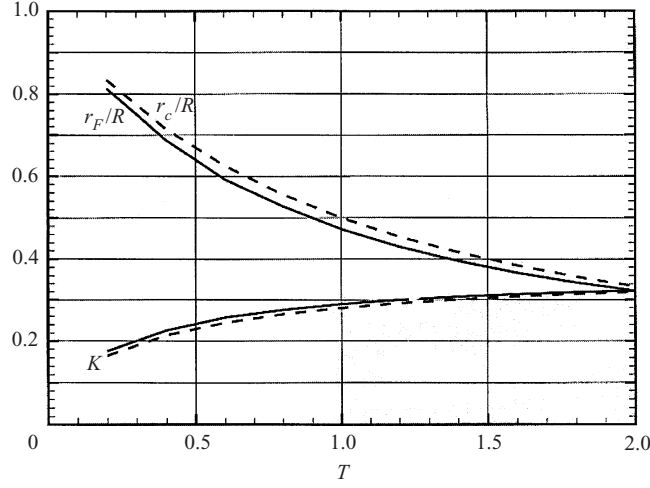
FIGURE 9. Theoretical prediction for the dependence of $K = (h/R)(N/f)$ (lower lines) and the dimensionless front position, r_F/R and r_c/R (upper lines), on the dimensionless time T. The lower solid line is deduced by volume matching, and the lower dashed line by setting $r_F = r_C$ of the initial conjecture.

where the coefficient is given by

$$C_1 = \frac{\Omega^2 R^2 H \bar{\rho}}{g \Delta \rho} = \frac{1}{4} \left(\frac{f}{N} \right)^2 R^2,$$

and we recall that $r_F \leqslant r \leqslant R$, $0 \leqslant S \leqslant 1$, $f = 2\Omega$ and $N^2 = g\Delta\rho/(\bar{\rho}H)$.

Equation (4.22) yields the height h of the corner region. Substituting the condition $S = 1$ at $r = R$ and appropriate values of T and $r_F(T)$ transforms (4.22) into the relationship

$$h = K(T) \left(\frac{f}{N} \right) R. \tag{4.23}$$

Ideally, the radius r_F where the interface (4.22) intersects the bottom ($z = 0$) is exactly the position of point C in figure 8, i.e. $r_F = r_C = R(1 + T)^{-1}$. This is a very good approximation in the present case, and moreover, provides an analytical result for h by straightforward substitution into the foregoing equations. However, the interface BC calculated by the kinematic condition (4.12) does not in general correspond precisely to that obtained from the dynamic pressure continuity condition (4.22). In order to deduce the front radius r_F, we must apply the global volume continuity condition between regions I and III. This continuity condition requires the numerical solution of (4.22) and numerical evaluation of the volume in the region below the interface. (Such a numerical calculation is also necessary in order to verify that the pressure continuity yields an acceptable result.)

The final results are summarized in figures 9 and 10. Figure 9 indicates the evolution of the coefficient K in (4.23) and the front position r_F with the scaled time,

$$T = 0.9 E^{1/2} \Omega \left(\frac{R}{h} \right) t = \frac{0.45}{K} E^{1/2} Nt. \tag{4.24}$$

The coefficient K increases with time, but only slightly (from 0.2 to 0.3) in the range $0.3 < T < 2$ pertinent to our investigation. Conversely, r_F^2 decreases substantially over
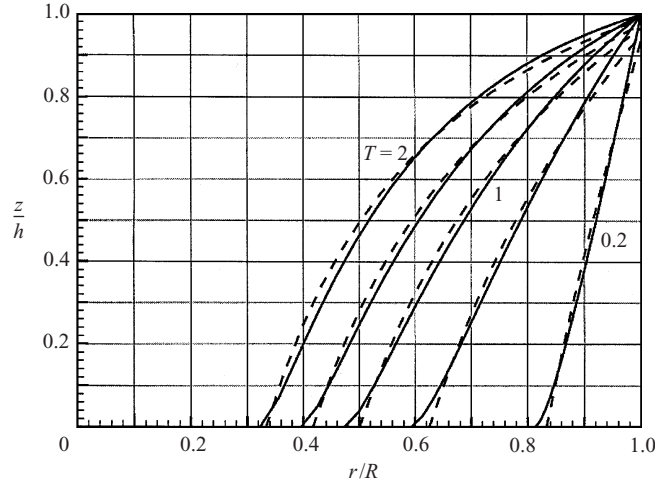
FIGURE 10. The model prediction for the shape of the interface BC between the core and corner regions. The solid line is deduced by volume matching, and the dashed line by setting $r_F = r_C$ of the initial conjecture. $T = 0.2, 0.6, 1.0, 1.4, 2.0$.

this time interval. This behaviour vindicates the assumption that h is quasi-constant and, moreover, is consistent with the experimental and numerical observations. We note that the calculation of K with the approximation $r_F = r_C$ (dashed lines) gives essentially the same results as the more sophisticated model. This provides important *a posteriori* justification of our initial conjecture (4.4)–(4.5).

Figure 10 indicates the predicted evolution of the shape of the interface defining the corner region. The solid line represents the interface provided by the dynamic pressure continuity conditions (4.23), while the dashed line represents the interface obtained from the kinematic manipulation of the flow in region I, (4.12). The agreement between the two is good, which again supports our initial conjecture.

We emphasize that the modelled flow field has been closed without the introduction of any adjustable parameters. This model provides useful information and insight into the spin-up process. In particular, it indicates that the influence of the boundary layers is restricted to the axial domains of thickness

$$h/R \approx 0.30(f/N) \tag{4.25}$$

adjacent to the solid horizontal boundaries, and that the time of effective action of these layers is $T = 2$, or in dimensional form

$$t \approx 1.3/(E^{1/2}N). \tag{4.26}$$

Thereafter, the boundary layer suction is restricted to a spot whose area is less than 10% that of the horizontal boundary. Outside this small area there is negligible contact between the non-rotating fluid and the horizontal boundary: a buffer zone of rotating fluid separates the non-rotating core from the rotating disk. Evidently, the elimination of the sharp boundary layers requires that the spin-up process enter a new, much slower stage.

The stratification of the non-rotating fluid in region I is significantly reduced during this progression. In the rotating corner regions a radial stratification appears that also has influence on the angular velocity, which consequently decays with z, as indicated by the last term on the right-hand side of (4.18).

4.4. *Momentum diffusion from the sidewall and other smoothing effects*

The diffusion of angular momentum from the sidewall is expected to be the most important effect in domain IV during the period of stable axisymmetric motion. This contribution can be readily estimated. We assume that the height of the container is (significantly) larger than the region affected by the Ekman layers, $H > h \approx 0.3(f/N)R$. When the curvature and endwall influences are negligible, the diffusion into the stationary interior may be described in terms of the classical 'Stokes first problem', that is, the flow driven by the impulsively started parallel motion of a plate in a fluid at rest. The result is

$$\omega(r, t) = \Omega \operatorname{erfc} \eta, \tag{4.27}$$

$$\eta = \frac{R - r}{2(vt)^{1/2}} = \frac{R - r}{2R} E^{-1/2}(\Omega t)^{-1/2}. \tag{4.28}$$

Defining by Δr the thickness of the sidewall layer when $\omega/\Omega \geqslant 0.03$ (i.e. $\eta \geqslant 3/2$), we obtain

$$\frac{\Delta r}{R} = 3E^{1/2}(\Omega t)^{1/2} \approx \sqrt{3}E^{1/4}(f/N)^{1/2}T^{1/2}, \tag{4.29}$$

after use of (4.7) and (4.23).

The result (4.29) indicates that the rotation of the cylindrical wall penetrates into a layer of thickness $\sim 2E^{1/4}R$ of region IV during the time interval ($T = 2$) in which the Ekman layer spins up region I. However, the diffusion effect and (4.29) are expected to be relevant for a considerably longer period than the Ekman spin-up time interval. The cyclostrophic–geostrophic balance (4.16)–(4.17) implies that the density readjusts: in the layer with significant ω a positive $\partial\rho/\partial r$ is expected to appear, i.e. the isopycnals move upwards near the cylindrical wall. Furthermore, after the decay of the Ekman layer influence, domain III (and what is left of I) become affected by diffusion of angular momentum from the bottom wall. The thickness of this diffusion layer in the centre region can also be estimated by (4.29) (with the proper interpretation of Δr as a vertical interval).

An inspection of the numerically computed angular velocity profiles in figures 6 and 7 confirms the predictions of the angular momentum diffusion from the sidewalls and bottom walls into the core.

The curved interface BC represents a discontinuity in angular velocity and density. In Wedemeyer's (1964) inviscid model of homogeneous spin-up from rest, the front between the rotating and non-rotating regions is also singular; however, because it is vertical, a relatively simple smoothing occurs there as shown by Venezian (1970; see also Hyun *et al.* 1983). Here the situation is more complicated. Across the curved interface BC the angular velocity jumps from $\omega > 0$ given by (4.18) in domain III to 0 in domain I. One anticipates the presence of an inclined boundary layer on this interface; however, this layer is expected to generate minimal transport relative to the bottom boundary layer since: (*a*) the jump in angular velocity is relatively small (we estimate at most 0.36Ω) owing to the 'thermal-wind'-type coupling between ρ and ω (see (4.18)) causing ω to decrease with z in the corner region, and (*b*) the vertical transport of fluid by the inclined boundary layer will be hindered by buoyancy effects. We therefore expect that this discontinuity makes a minor contribution to the flow field during the time of formation of the corner region, but will become progressively more significant as the spin-up proceeds. This additional region of friction enhances angular momentum transport and hence the trend is to accelerate the spin-up process. Details of this complex boundary region are left as a challenge for future study.
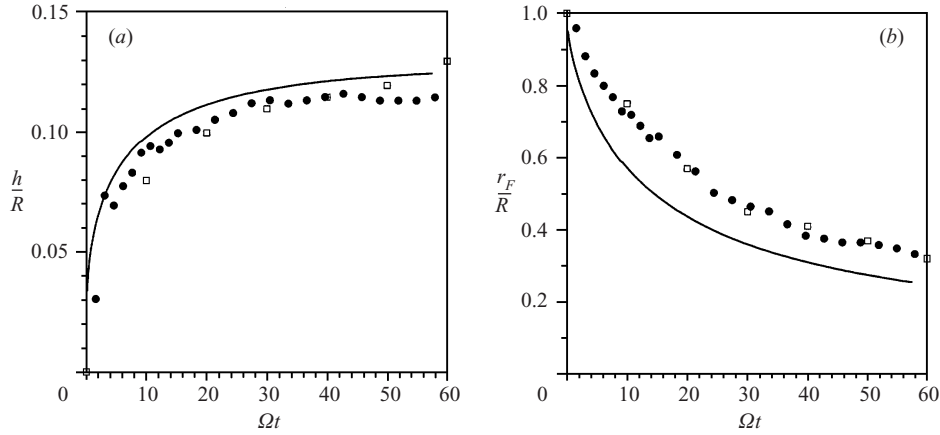
FIGURE 11. The observed and predicted evolutions of (*a*) the dimensionless height h/R of the corner regions and (*b*) the dimensionless radius of the front r_F/R for experiment A (for which $f/N = 0.61$ and $\Omega = 0.305\,\text{s}^{-1}$). Dots denote experimental observations, squares denote results from the numerical simulations, and the line represents predictions from the theoretical model.
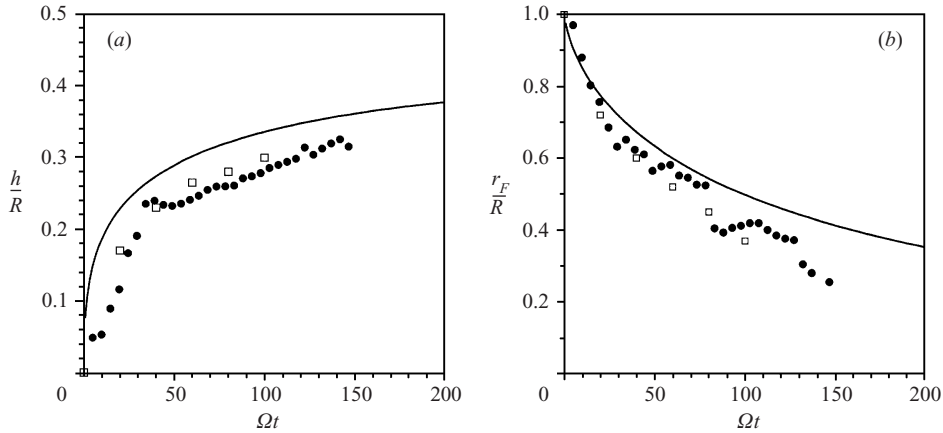

FIGURE 12. The observed and predicted evolutions of (*a*) the dimensionless height h/R of the corner regions and (*b*) the dimensionless radius of the front r_F/R for experiment B (for which $f/N = 1.21$ and $\Omega = 1.02\,\text{s}^{-1}$). Dots denote experimental observations, squares denote results from the numerical simulations, and the line represents predictions from the theoretical model.

The horizontal interface *AB* between domains I and IV bears a discontinuity of the shear $\partial u/\partial z$ of magnitude $E^{1/2}\Omega r/h$. This discontinuity will also be smoothed out according to $\partial u/\partial t \approx \nu \partial^2 u/\partial z^2$. Straightforward analysis (see Ungarish & Greenspan 1984, Appendix) indicates the formation of a weak layer of thickness $O[(E\Omega t)^{1/2}]$: the layer attains a thickness of $O(E^{1/4})$ in the period of interest. The resulting contribution to the corner flow during the first spin-up stage is negligible. A similar mechanism tends to smooth out density gradients but, in view of the large Schmidt number, such effects will have a negligible impact on the transport of angular momentum.

5. Comparison of experimental, numerical and model results

Figures 11 and 12 show the comparison of the model predictions for the evolution of the height and radius of the corner region with our numerical and experimental
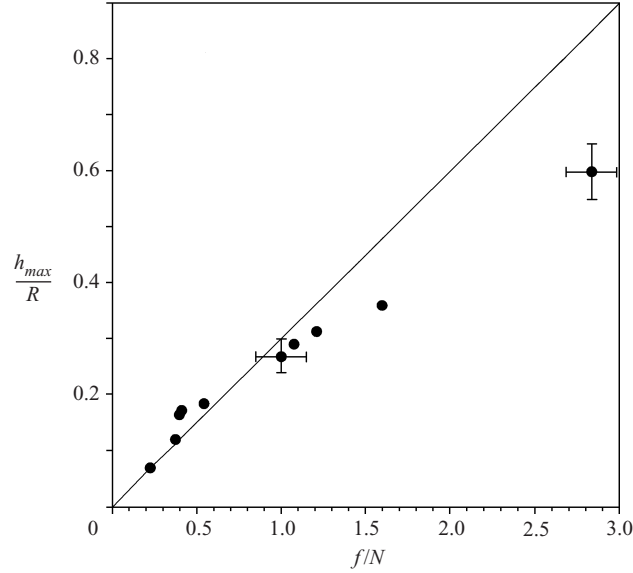
FIGURE 13. The observed and theoretically predicted dependence of the dimensionless maximum corner height h_{max}/R on f/N. Dots denote experimental observations, and the line represents predictions from the theoretical model. Characteristic error bars are shown.

results. Figure 11 represents the case $f/N < 1$ (experiment A) and figure 12 the case $f/N > 1$ (experiment B). In the latter case, the mixing above the interface due to the aforementioned baroclinically unstable wave motions (that set in at a time $\Omega t \approx 30$) is neglected in the experimental measurements of h, i.e. h is the height of the grey corner region at the sidewall of the tank evident in figure 4 at $\Omega t = 60$. In both cases, the qualitative agreement is excellent and the quantitative agreement is quite reasonable. The model slightly overpredicts the value of h, thus indicating that the idealized spin-up process is slightly more efficient than the real one. There are several reasons for this discrepancy.

First, in the model calculation of h we have neglected viscous effects apart from those responsible for the Ekman layers. A viscous layer of increasing thickness appears near the cylindrical wall (see §4.4), which necessarily affects the local pressure distribution and so the shape of the upper tip of the corner region III. Moreover, one expects that viscous effects will tend to smooth out the difference of angular velocity between regions I and III and so alter the local pressure distribution and corner shape. We note that similar discrepancies between idealized and real flow arise in the relatively simple problem of spin-up of a homogeneous fluid (Wedemeyer 1964; Weidman 1976*a,b*; Hyun *et al.* 1983). However, in the stratified case under consideration, there are additional diffusive effects connected with the density jumps at the interface. The net contribution of these neglected viscous and diffusive mechanisms is expected to hinder the development of the corner region and smooth its interface with the interior core region. Second, the pressure balances used to describe regions I and III are strictly correct only in the asymptotic sense of both $E^{1/2}R/h$ and $\Delta\rho/\bar{\rho} \to 0$. Third, our model is again only the 'first iteration' in a virtual trial-and-error process, and some of the initial postulates need correction, for example the assumption that h is time-independent. As we were unable to perform any straightforward corrections, we leave this topic open for further study.
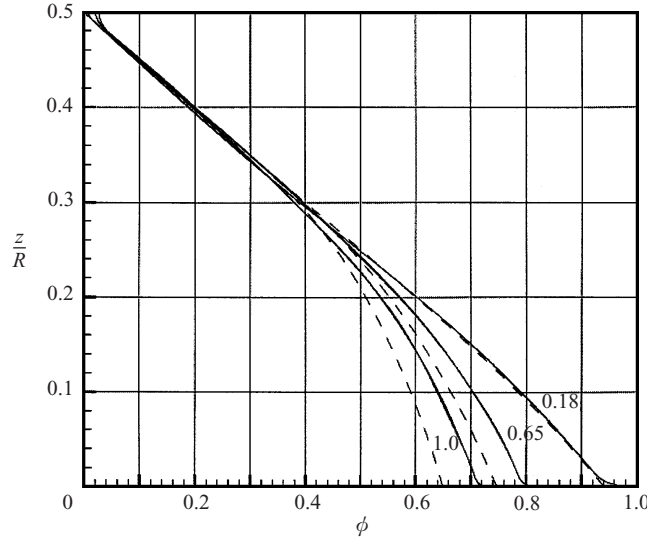
FIGURE 14. The evolution of the vertical profile of the density function ϕ (defined in (3.1)) in region I for experiment B. Solid lines denote the results of our numerical simulations, and the dashed lines denote the predictions of our theoretical model. The profiles at three dimensionless times, $\Omega t = 0.18$, 0.65 and 1.0, are shown.

Figure 13 shows the dependence of the maximum height attained by the corner region on f/N in several experiments. The results are well-described by the straight line corresponding to $K = 0.3$ in (4.23). For $f/N < 1.5$, the corner height attains a maximum value, h_{max}, at a time $t \approx 1.3/(E^{1/2}N)$. The point corresponding to $f/N = 1.2$ was taken at $t \approx 1.3/(E^{1/2}N)$, when baroclinic wave motions began to develop above the core region. For larger values of f/N the onset of asymmetric instability of the core region was initiated prior to the maturation of the corner region; consequently, the corner heights could not be clearly measured.

Figure 14 shows a comparison between the model predictions and numerical simulations of density profiles in the central non-rotating core for experiment B. At any given time, the numerical profiles for various r collapse onto one line, which confirms that the density is dependent only on z and t, as predicted by the model. Both the numerical and theoretical models indicate that the stratification is reduced with time in the region $z/R < 0.3f/N$, but remains practically unaltered for larger values of z. The decay predicted by the model is again slightly faster than the numerical result; nevertheless, the qualitative agreement is excellent.

The evolution of the total angular momentum yields valuable insight into the adjustment process accompanying spin-up from rest. We consider the variable

$$\Gamma(t) = 2\pi \int_0^H dz \int_0^R \omega r^3 dr, \tag{5.1}$$

noting that $\Gamma(\infty) = 0.5\pi\Omega R^4 H$. From the results of our theoretical model, we calculate in turn the contributions to Γ from the corner regions (see (4.18)) and the sidewall layer ($\approx 2\pi\Omega R^4(H - h)(E\Omega t)^{1/2}$, see (4.27)). The scaled results, $\Gamma(t)/\Gamma(\infty)$, are presented in figure 15. The agreement between the theoretical and the numerical results is good. To facilitate interpretation, we also display the connection between Ωt and the scaled times T and $\tau = t/\tau_{su}$ (the homogeneous spin-up times, τ_{su}, are $118\Omega^{-1}$ and $258\Omega^{-1}$ for cases A and B, respectively).
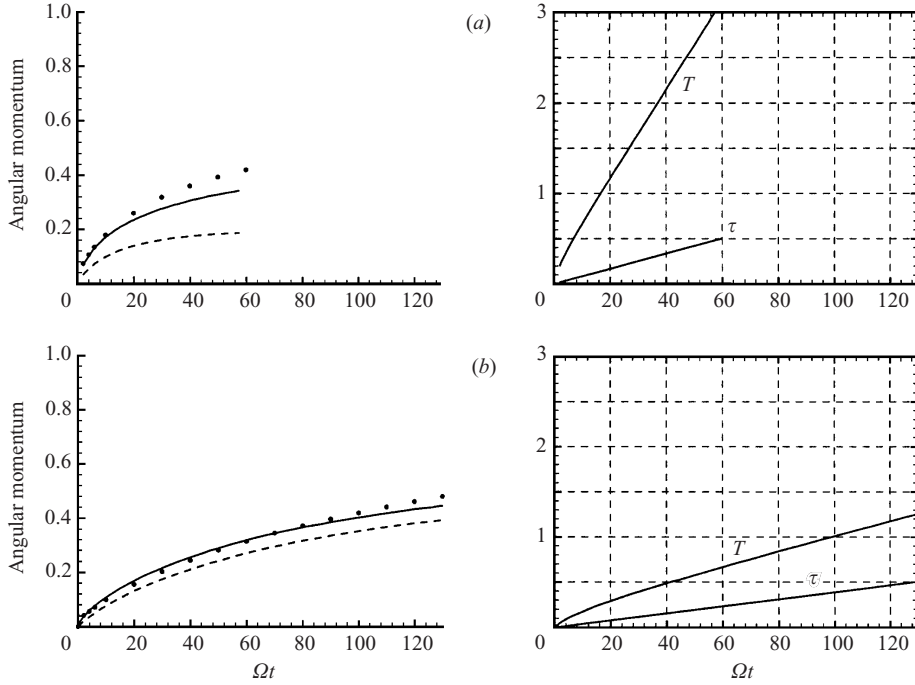
FIGURE 15. The total scaled angular momentum $\Gamma(t)/\Gamma(\infty)$ as a function of Ωt: numerical simulations (dotted curve) and model predictions encorporating the bottom boundary layer (dashed curve) and bottom boundary plus sidewall layers (solid curve) for cases (*a*) A and (*b*) B. The plots on the right-hand side show T and τ as functions of Ωt.

For a homogeneous fluid, Wedemeyer's (1964) model predicts $\Gamma(t)/\Gamma(\infty) = 1 - \exp(-2\tau)$. Cases A and B are displayed for values of τ up to approximately 0.5; in the absence of stratification, one expects Γ to reach $0.6\Gamma(\infty)$ in this time. Evidently, the stratification significantly hinders the readjustment process in both cases. We also note that the contribution of the sidewall to the production of angular momentum ultimately becomes significant in case A, but remains very small in case B. This is a consequence of the fact that case A has a stronger stratification (N/f) and a larger viscosity (E) than case B. Therefore, in case A the corner layer covers the bottom after a relatively short Ωt period, and the sidewall layer spreads relatively rapidly. The different parameter regimes characterizing cases A and B are similarly reflected in the total spin-up times T. We emphasize that the good agreement between the numerical predictions and the theoretical model provides validation for the assumed form of the angular velocity (4.18).

Another interesting spin-up diagnostic is the frictional torque applied by the bottom boundary layer,

$$M = -2\pi E \int_0^1 \left(\frac{\partial \omega}{\partial z}\right)_{z=0} r^3 \mathrm{d}r, \qquad (5.2)$$

where lengths are scaled with R, velocity with ΩR and force with $\bar{\rho}\Omega^2 R^4$. This quantity is straightforwardly calculated from the numerical computations. Moreover, for the model we note that M must be equal to the rate of angular momentum flux out from
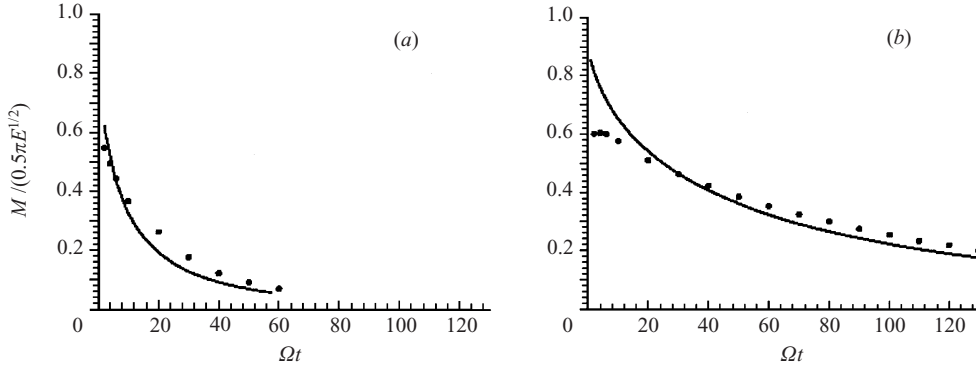
FIGURE 16. The scaled bottom boundary layer torque $M/(0.5\pi E^{1/2})$ as a function of Ωt: numerical (dotted curve) and model (solid curve) predictions for cases (*a*) A and (*b*) B.

the boundary layer (at $z = 0^+$),

$$M = 2\pi \int_{r_F}^1 (w\omega)_{z=0^+} r^3 \mathrm{d}r = 0.5\pi \times 0.9 E^{1/2} r_F^2, \tag{5.3}$$

where (4.18) has been used (here w is independent of r and simply related by continuity to (4.1)). The evolution of M, as predicted by the numerical computations and the model, is shown in figure 16. In the numerical results the initial formation of the boundary layers during $\Omega t \leqslant 10$ is evident (see figures 3*b* and 4*b*). Thereafter, the agreement between the numerical and model results is good, and the differences between cases A and B are well-captured by the model. The faster decay of the torque in the more stratified case A is evident. Since M is expected to be a relatively sensitive diagnostic of the boundary layer dynamics, this agreement between theory and numerics further validates the Wedemeyer-type boundary layer approach employed in our model, in particular (4.18).

The fact that the analytical predictions for case A are meaningful and in fair agreement with the numerical results indicates that the model is a robust tool. In this case the (dimensionless) thickness of the corner layer $h/R \approx 0.1$ is only about five times larger than the thickness of the Ekman layer $3E^{1/2} = 0.02$; moreover, $E^{1/4} = 0.09$ is not really small, and hence the possibility of large errors could not be excluded *a priori*. Another encouraging feature is the good agreement at early times, even for $\Omega t \approx 10$ (less than two revolutions of the container), at which time the Ekman layers and corner region are barely developed.

Figures 15 and 16 show consistent behaviour: in both cases, the model slightly over- and underpredicts the effectiveness of the spin-up at, respectively, early and later times. The discrepancy at early times reflects the fact that the model does not take into account the time of formation of the Ekman layer and of the corner region. At later times, the internal flow is affected by the viscous effects which have not been incorporated in the model, specifically those discussed in §4.4.

Finally, we remark that when $H/R < 0.3f/N$ the height of the corner region exceeds the half-height of the container, H. This situation has indeed been observed in our experiments, and involves the interaction of fluid from the top and bottom corner regions at the midplane. The present theoretical model cannot adequately describe this case because it is based on the assumption that $h < H$.

6. Conclusions

Our experimental study of stratified spin-up from rest in a cylinder indicates that the flow is always characterized by an initial axisymmetric stage governed by boundary layer transport. By virtue of its axisymmetry, this initial stage is readily amenable to numerical and theoretical analysis; consequently, we have supplemented our laboratory study with numerical simulations and analytical models in order to obtain a quantitative description of the flow.

Stratified spin-up from rest may be most easily described in terms of figure 8. Rotation prompts the establishment of horizontal boundary layers (region II) that transport fluid radially from the stratified core (region I) towards the corners of the tank. The resulting secondary $O(E^{1/2})$ meridional flow is confined by the stratification to a corner region (III) of height $h \approx 0.3Rf/N$. In domain IV, the fluid remains largely unperturbed by the boundary motion: its initial stratification and quiescence are maintained everywhere except within the sidewall boundary layer. The core and corner regions shrink and expand, respectively, until a time $1.3/(E^{1/2}N)$, after which the corner region covers the bulk of the bottom surface and the sidewall boundary layer in region IV has a thickness of $O(E^{1/4}(f/N)^{1/2}R)$. While the stratification within region IV persists, that in region I is necessarily reduced by the boundary layer transport. Moreover, the progressive decrease in density of the fluid injected into the lower corners produces a radial density gradient in region III. Finally, the interface between regions I and III is prescribed by pressure continuity between the quiescent, vertically stratified core region and the rotating, radially stratified corner region.

After this initial stage of spin-up, a substantial volume of non-rotating core fluid persists, shrouded from the container boundaries by buffer regions of rotating fluid. The initially sharp gradients of angular velocity are thus smoothed, and boundary layer transport is no longer an effective means by which to transfer angular momentum from the container walls. The subsequent evolution requires a separate investigation, for which the present study provides the initial conditions.

The details of the flow field in the proximity of the bowed moving interface between the corner region (III) and the core (I) remain a challenge for future investigation. The resolution in both our theoretical and numerical models is insufficient to elucidate the interplay between the strong velocity and density gradients in this region, which may cause local mixing and instability.

The spin-up from rest of a stratified fluid is markedly different from that in a homogeneous fluid, where the interface between regions I and III is vertical and region IV does not exist. Our model captures the steepening of the interface between rotating and stationary fluid regions with increasing f/N, but cannot recover the homogeneous case in the $N \rightarrow 0$ limit because the model is based on the assumption that h is smaller than the container half-height H. When $H/R < 0.3f/N$, this assumption is violated: the corner regions in the upper and lower halves of the container meet, and region IV vanishes. In the unstratified case, the spin-up time is $2H/(E^{1/2}R\Omega)$. In the stratified case, the corner regions are fully developed, and the boundary layer transport suppressed, after a time $1.3E^{1/2}/N$. The spin-up time of the entire fluid domain is not yet readily discernible, and will depend explicitly on the form of the subsequent flow evolution.

It is valuable to compare the nonlinear spin-up from rest considered here to linear incremental spin-up, in which the container boundary is increased instantaneously from a value $\Omega - \Delta\Omega$ to Ω and $|\Delta\Omega|/\Omega \ll 1$ (e.g. Walin 1969). In the linear case, the bulk interior possesses initial vertical vorticity which is stretched by the Ekman
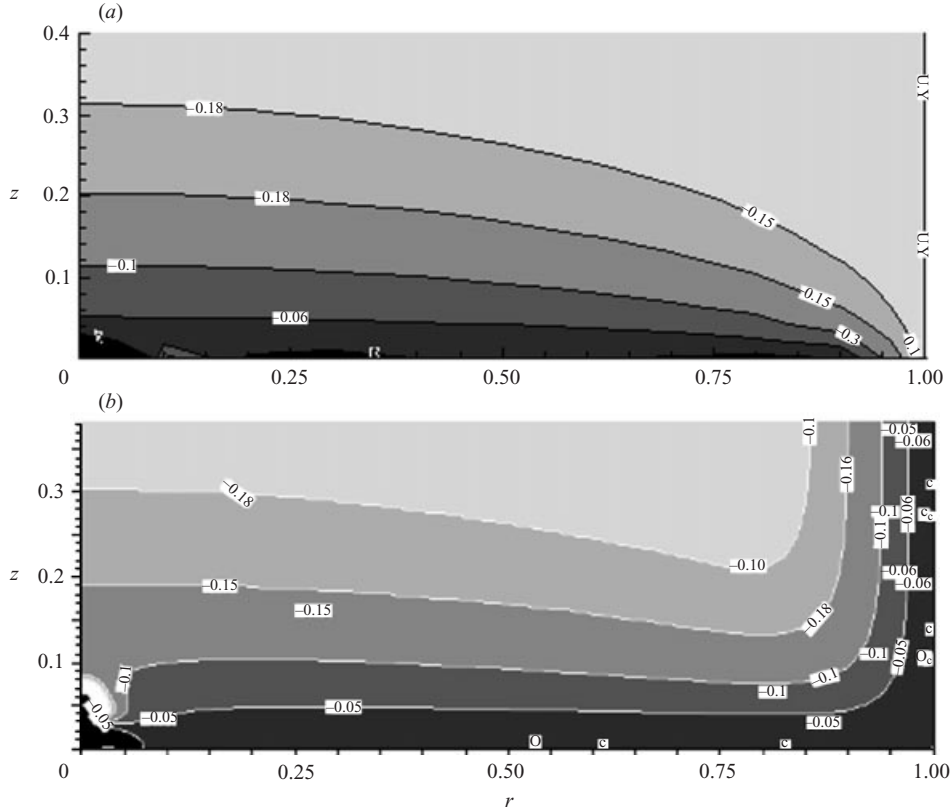
FIGURE 17. Contour plots of angular velocity for data like experiment A but with $Ro = 0.2$, at $\Omega t = 60$: (a) calculated from Walin's (1969) relation (1.2) obtained for linear spin-up and (b) numerical simulation including the influence of the sidewall boundaries.

suction into the shear layers on the solid boundaries. Nevertheless, the stratification similarly limits the vertical transport from the horizontal boundaries and leads to the formation of recirculating domains (with vertical extent prescribed by f/N) which separate the stratified core from the horizontal boundaries. The Ekman layer spin-up effects influence the fluid in these buffer domains, but the remaining core fluid remains essentially at its initial angular velocity during this process.

Walin's results (see also Buzyna & Veronis 1971) indicate that in the case of linear stratified spin-up, to the lowest mode, the domain affected by Ekman circulation has a thickness of approximately $0.26 f/N$ in the centre of the tank, and characteristic spin-up timescale $0.52/(E^{1/2}N)$. These scales are in good agreement with the results derived here, (4.25) and (4.7), for spin-up from rest. The difference with spin-up from rest, however, appears in the shape of the zone influenced by the Ekman layer. Figure 17(a) displays this shape calculated with Walin's result for linear spin-up for Rossby number $Ro = |\Delta\Omega|/\Omega = 0.2$ and the same parameters as experiment A at $\Omega t = 60$; for comparison, the numerical simulation that encorporates spin-up by the sidewall boundaries is shown in figure 17(b). The spun-up region near the horizontal boundary is dome-shaped with maximal thickness in the centre and zero thickness near the rim of the tank. The Ekman-layer circulation displaces fluid towards the centre, and due to the initial angular momentum, which is stretched in the Ekman layer near the centre of the tank, a dome-shaped domain of spun-up fluid appears. This is

in contrast with spin-up from rest, where there is a clear-cut connection between changes in density and angular velocity: the fluid acquires angular momentum by being flushed through the lower boundary layer, and accumulates in the corner region.

Finally, we note that there have been no reported observations of core instability in the linear problem, which is suggestive of the gyroscopic stability imparted to the core by the background rotation. Our experiments indicate that, when $f/N > 1$, the axisymmetry of the flow is broken by baroclinically unstable waves propagating along the interface between regions I and III. It is noteworthy that similar non-axisymmetric waves were observed at the interface in the differential spin-up of a two-layer fluid system (Linden & van Heijst 1984). In our study, the breaking of the waves generated mixing above the interface of the corner region, and obscured our measurements of the corner height. Nevertheless, provided the waves broke after the maturation time of the corner regions, $1.3/(E^{1/2}N)$, the corners achieved the maximum height, $0.3Rf/N$, predicted by our theoretical model. Conversely, for large f/N, the wave breaking prompted instability of the central core prior to the maturation of the corner regions, which thus do not attain their maximum height.

Our observations indicate that the subsequent evolution of the flow depends critically on two parameters that characterize the non-rotating core that persists following the decay of the boundary layer transport, specifically the aspect ratio of the core H_c/R_c and f/N_c. We note that both parameters are uniquely determined by the initial flow stage elucidated herein: the geometry of the core region is prescribed by that of the corner regions, and the stratification within the core N_c reflects the degree of stretching of isopycnals by the vertical transport into the horizontal boundary layers. Our study thus provides the framework for further experimental, numerical and theoretical investigations of spin-up from rest of a stratified fluid, which will be the subject of a forthcoming paper.

Appendix. The finite-difference code

Consider the time advance of a flow-field variable denoted by a at time t to the new value denoted by a^+ at time $t + \delta t$. We use a forward-time, finite-difference technique. One time step for the momentum equation (3.3) with the Coriolis and pressure terms treated implicitly and other terms treated explicitly yields

$$\boldsymbol{v}^+ + 2\delta t\hat{\boldsymbol{z}} \times \boldsymbol{v}^+ = -\frac{\delta t}{1+\gamma\phi}\nabla p^+ + \delta t\boldsymbol{X} + \boldsymbol{v} \equiv \boldsymbol{B}, \qquad (A\,1)$$

where

$$\boldsymbol{X} = -\boldsymbol{v}\cdot\nabla\boldsymbol{v} + \frac{1}{1+\gamma\phi}[(\gamma r\hat{\boldsymbol{r}} - \mathscr{F}^{-2}\hat{\boldsymbol{z}})\phi + E\nabla^2\boldsymbol{v}]. \qquad (A\,2)$$

With some simple vector algebra manipulations (as discussed in detail by Ungarish 1993, p. 303), we obtain from (A 1) an explicit expression for $\boldsymbol{v}^+$,

$$\boldsymbol{v}^+ = \frac{1}{1+4\delta t^2}[\boldsymbol{B} + 4\delta t^2(\hat{\boldsymbol{z}}\cdot\boldsymbol{B})\hat{\boldsymbol{z}} - 2\delta t\hat{\boldsymbol{z}}\times\boldsymbol{B}]. \qquad (A\,3)$$

We next apply the divergence operator to both sides of this expression and impose the continuity equation (3.2) on $\boldsymbol{v}^+$. The result is an elliptic equation for the pressure p^+ at $t + \delta t$,

$$\nabla \cdot \frac{1}{1 + \gamma\phi}\nabla p^+ + 4\delta t^2 \frac{\partial}{\partial z}\frac{1}{1 + \gamma\phi}\frac{\partial p^+}{\partial z} - \nabla \cdot X - 4\delta t^2 \frac{\partial}{\partial z}\hat{z} \cdot X$$

$$- 2\delta t\hat{z} \cdot \nabla \times X - 4\delta t\frac{\partial w}{\partial z} - 2\hat{z} \cdot \nabla \times \boldsymbol{v} - \frac{\nabla \cdot \boldsymbol{v}}{\delta t} = 0. \quad (A\,4)$$

(Theoretically the last term on the left-hand side is zero, but to prevent accumulation of numerical errors it is sometimes useful to keep it in the calculations.) The boundary conditions for (A 4) are of Neumann type, provided in terms of $\hat{\boldsymbol{n}} \cdot \nabla p^+$ by the velocity boundary conditions, and $p^+ = 0$ is set at some point for uniqueness. Hence the solution p^+ is well-defined. Using it, we can straightforwardly obtain the velocity field $\boldsymbol{v}^+$ from (A 3). The ϕ^+ field can be calculated next using the scalar equation (3.4). This completes, in principle, the time step advance, and a new cycle can be attempted. The accuracy of the time discretization is $O(\delta t^2)$.

The spatial discretization is performed on a staggered grid as sketched in figure 5. The variables p and ϕ are defined at mid-cell position denoted (i, j); u and v are both defined at the positions $(i \pm \frac{1}{2}, j)$ (to allow straightforward implementation of the Coriolis coupling) and w is defined at $(i, j \pm \frac{1}{2})$. Both the r and z grid coordinates may be stretched by simple mapping functions $r(\mathscr{R})$ and $z(\mathscr{Z})$. The grids $\mathscr{R}_i = (i + \frac{1}{2})\delta\mathscr{R}$ and $\mathscr{Z}_j = (j + \frac{1}{2})\delta\mathscr{Z}$ are uniform in the domain $(0 \leqslant \mathscr{R} \leqslant R, 0 \leqslant \mathscr{Z} \leqslant H)$ with intervals $\delta\mathscr{R} = R/il$ and $\delta\mathscr{Z} = H/jl$. The truncation error is $O(\delta\mathscr{R}^2 + \delta\mathscr{Z}^2)$. Dummy cells are added for easy implementation of boundary conditions. An illustration of the finite-difference approach is

$$\left(\frac{1}{r}\frac{\partial}{\partial r}r\frac{1}{1 + \gamma\phi}\frac{\partial p}{\partial r}\right)_{r_i, z_j} = \frac{1}{r_i}\frac{1}{r_i'\delta\mathscr{R}}(Y_{i+1/2, j} - Y_{i-1/2, j}), \quad (A\,5)$$

where

$$Y_{i+1/2, j} = r_{i+1/2}\frac{1}{1 + \gamma\phi_{i+1/2, j}}\frac{1}{r_{i+1/2}'\delta R}(p_{i+1, j} - p_{i, j}) \quad (A\,6)$$

and r_i' is the derivative of $r(\mathscr{R})$ at $\mathscr{R}_i$ (substituting $i - 1$ in place of i yields $Y_{i-1/2, j}$).

This method of central differences was employed for all terms, except for the advection terms in transport equation (3.4). This equation needs special attention because when the diffusion coefficient is set to 0 the interface between the corner region and the core is a moving discontinuity (kinematic shock) of the density field $\phi(r, z, t)$, and even with the physical value of E/σ attempting straightforward numerical computation of this region is problematic. An accepted and well-documented numerical mean for capturing such shocks in 2–3 grid intervals without introducing spurious oscillations in the entire flow field, is the 'artificial diffusion', used in conjunction with a special predictor–corrector scheme proposed by Anderson, Tannehill & Pletcher (1984, p. 28). This method has been successfully used for a related spin-up from rest problem by Amberg & Ungarish (1993). Thus, for the density transport equation, following Anderson *et al.*'s explicit method, we used at each time step the

Run	il	jl	a	H	E	$E^{1/2}/$(first z interval)
A	200	150	2.5	0.43	5.25×10^{-5}	2.95
B	100	300	2.5	0.50	1.50×10^{-5}	3.10

TABLE 2. Typical grids for computations A and B.

predictor–corrector relationships

$$\left. \begin{aligned}
\phi_{i,j}^p &= \phi_{i,j} - \delta t (Adv_f \phi)_{i,j}^f + \delta t (Dif\,\phi)_{i,j}, \\
\phi_{i,j}^c &= \phi_{i,j}^p - \delta t (Adv_b \phi^p)_{i,j} + \delta t (Dif\,\phi^p)_{i,j}, \\
\phi^+ &= 0.5(\phi_{i,j} + \phi_{i,j}^c),
\end{aligned} \right\} \tag{A7}$$

where Adv_f and Adv_b denote the advection terms as approximated by forward and backward differencing, and Dif denotes the diffusion terms approximated by central differences.

Since our diffusion coefficient is $E/10 \sim 10^{-6} < (\delta r^2 + \delta z^2) \sim 10^{-4}$, the contribution of the artificial diffusion in regular flow regions (including the Ekman layer) is very small, like the original truncation error. Conversely, we can justify the use of artificial diffusion as follows. Assume that the original fluid in the physical system with $\sigma = 700$ is replaced by one with $\sigma = 10$, and that all other parameters are unchanged. In the time interval considered in this study no observable differences between the spin-up of the two fluids will be apparent (except in the interface region which cannot be resolved numerically in either case). The addition of small $O(\delta r^4 + \delta z^4)$ fourth-order derivative artificial dissipation terms in the momentum equations improved the numerical stability.

The combination of the foregoing time and space discretizations are the core of the computer code used in this work. For each time step the discretized form of the Poisson equation (A4) for the discretized variables $p_{i,j}^+$, $1 \leqslant i \leqslant il$, $1 \leqslant j \leqslant jl$ must be solved. This yields, after the implementation of the boundary conditions, a block tri-diagonal linear system; for uniqueness we impose $p_{1,1}^+ = 0$. The linear system was solved by a bi-conjugate gradient iterative algorithm (Press *et al.* 1992). The $p_{i,j}$ field provides the starting values in the iteration for $p_{i,j}^+$. The computations use real-8 variables. The typical grid has $il = 200$ constant radial intervals and $jl = 150$ stretched axial intervals, with $z_1' \approx 0.7$ and $z_{jl}' \approx 1.4$. At least 3 axial intervals were contained within the Ekman length $E^{1/2}$ and hence the estimated resolution of the volume transport in this region is better than 1%. The typical time step was $\delta t = 2 \times 10^{-3}$ and determined mainly by numerical stability considerations. The accumulated time-discretization error after n time steps, estimated as $n\delta t^2$, was typically less than 1%. In several test cases the grid intervals and the time step were changed, without causing any significant differences in the results.

The bi-conjugate gradient method performed typically 200 iterations per time step to reach the allowed error $\varepsilon = 10^{-5}$, where ε is the Euclidean seminorm of the residues divided by the seminorm of the right-hand side of the system of equations. The typical average relative error, $\varepsilon/(il \times jl)$, in the solution of $p_{i,j}^+$ is therefore less than 10^{-9}.

To be more specific, the stretching function used is

$$z = H(a^{\mathscr{Z}} - 1)/(a^H - 1), \tag{A8}$$

where $a > 0$ is prescribed and the length is scaled with R. Both the physical grid z and the uniform grid $\mathscr{Z}$ are in the range $[0, H]$, $\mathscr{Z}_j = (j - 0.5)\delta\mathscr{Z}$ and $\delta\mathscr{Z} = H/jl$. More details are given in table 2.

REFERENCES

AMBERG, G. & UNGARISH, M. 1993 Spin-up from rest of a mixture: simulation and theory. *J. Fluid Mech.* **246**, 443–464.

ANDERSON, D. A., TANNEHILL, J. C. & PLETCHER, R. M. 1984 *Computational Fluid Mechanics and Heat Transfer.* Hemisphere.

ANDERSON, D. L. T. & GILL, A. E. 1975 Spin-up of a stratified ocean, with applications to upwelling. *Deep-Sea Res.* **22**, 583–595.

BAKER, E. T. 1995 Characteristics of hydrothermal discharge following a magmatic intrusion. In *Hydrothermal Vents and Processes.* Geol. Soc. Spec. Pub. 87, pp. 65–76.

BEARDSLEY, R. C., SAUNDERS, K. D., WARN-VARNAS, A. C. & HARDING, J. M. 1979 An experimental and numerical study of the secular spin-up of a thermally stratified rotating fluid. *J. Fluid Mech.* **93**, 161–184.

BLUMSACK, S. L. 1972 The transverse circulation near a coast. *J. Phys. Oceanogr.* **2**, 34–40.

BORMANS, M. 1992 An experimental study on the formation and survival of stratified subsurface eddies. *J. Geophys. Res.* **97**, 20155–20167.

BUZYNA, G. & VERONIS, G. 1971 Spin-up of a stratified fluid: theory and experiment. *J. Fluid Mech.* **50**, 579–608.

DEWAR, W. K., RHINES, P. B. & YOUNG, W. R. 1984 The nonlinear spin-up of a stratified ocean. *Geophys. Astrophys. Fluid Dyn.* **30**, 169–77.

DUCK, P. W. & FOSTER, M. R. 2001 Spin-up of homogeneous and stratified fluids. *Annu. Rev. Fluid Mech.* **33**, 231–263.

DUCK, P. W., FOSTER, M. R. & HEWITT, R. E. 1997 On the boundary layer arising of a stratified fluid in a container with sloping walls. *J. Fluid Mech.* **335**, 233–259.

GREENSPAN, H. P. 1968 *The Theory of Rotating Fluids.* Cambridge University Press.

GREENSPAN, H. P. 1981 A note on the spin-up from rest of a stratified fluid. *Geophys. Astrophys. Fluid Dyn.* **15**, 1–5.

GREENSPAN, H. P. & HOWARD, L. N. 1963. On a time dependent motion of a rotating fluid. *J. Fluid Mech.* **17**, 385–404.

HEWITT, R. E., DAVIES, P. A., DUCK, P. W. & FOSTER, M. R. 1999 Spin-up of stratified rotating flows at large Schmidt number: experiment and theory. *J. Fluid Mech.* **389**, 169–207.

HOLTON, J. R. 1965 The influence of viscous boundary layers on transient motion in a stratified rotating fluid, Part I. *J. Atmos. Sci.* **22**, 402–411.

HYUN, J. M. 1983 Axisymmetric flows in spin-up from rest in of a stratified fluid in a cylinder. *Geophys. Astrophys. Fluid Dyn.* **23**, 127–141.

HYUN, J. M., FOWLIS, W. W. & WARN-VARNAS, A. 1982 Numerical solutions for the spin-up of a stratified fluid. *J. Fluid Mech.* **117**, 71–90.

HYUN, J. M., LESLIE, F., FOWLIS, W. W. & WARN-VARNAS, A. 1983 Numerical solutions for spin-up from rest in a cylinder. *J. Fluid Mech.* **127**, 263–281.

LINDEN, P. F. & VAN HEIJST, G. J. F. 1984 Two layer spin-up and frontogenesis. *J. Fluid Mech.* **143**, 69–94.

MACCREADY, P. & RHINES, P. B. 1991 Buoyant inhibition of Ekman transport on a slope and its effect on stratified spin-up. *J. Fluid Mech.* **223**, 631–661.

MANLEY, T. O. & HUNKINS, H. 1985 Mesoscale eddies of the arctic ocean. *J. Geophys. Res.* **90**, 4911–4930.

MCWILLIAMS, J. C. 1985 Submesoscale, coherent vortices in the ocean. *Geophys. Rev.* **23**, 165–182.

PEDLOSKY, J. 1967 The spin-up of a stratified fluid. *J. Fluid Mech.* **28**, 463–479.

PEDLOSKY, J. 1968 An overlooked aspect of the wind-driven ocean circulation. *J. Fluid Mech.* **32**, 609–621.

PRESS, W. H., FLANNERY, B. P., TEUKOLSKY, S. A. & VETTERLING, W. T. 1992 *Numerical Recipes in Fortran.* Cambridge University Press.

SAKURAI, T. 1969 Spin down problem of rotating stratified fluid in thermally insulated circular cylinders. *J. Fluid Mech.* **37**, 689–699.

SPENCE, G. S. M., FOSTER, M. R. & DAVIES, P. A. 1992 The transient response of a contained rotating stratified fluid to impulsively started surface forcing. *J. Fluid Mech.* **243**, 33–50.

ST-MAURICE, J.-P. & VERONIS, G. 1975 A multi-scaling analysis of the spin-up problem. *J. Fluid Mech.* **68**, 417–445.

UNGARISH, M. 1993 *Hydrodynamics of Suspensions.* Springer.

UNGARISH, M. & MANG, J. 2003 The flow field and bare-spot formation in spin-up from rest of a two-layer fluid about a vertical axis. *J. Fluid Mech.* **474**, 117–145.

UNGARISH, M. & GREENSPAN, H. P. 1984 On the radial filling of a rotating cylinder. *J. Fluid Mech.* **141**, 97–107.

VENEZIAN, G. 1970 Nonlinear spin-up. *Top. Ocean Engng* **2**, 87–96.

WALIN, G. 1969 Some aspects of time-dependent motion of a stratified rotating fluid. *J. Fluid Mech.* **36**, 289–307.

WEDEMEYER, E. H. 1964 The unsteady flow within a spinning cylinder. *J. Fluid Mech.* **20**, 383–399.

WEIDMAN, P. D. 1976a On the spin-up and spin-down of a rotating fluid. Part 1. Extending the Wedemeyer model. *J. Fluid Mech.* **77**, 685–708.

WEIDMAN, P. D. 1976b On the spin-up and spin-down of a rotating fluid. Part 2. Measurements and stability. *J. Fluid Mech.* **77**, 709–735.